INTRODUCTION | FEBRUARY 07 2022

Overview of the MOSAiC expedition: Physical oceanography

Collections: Knowledge Domain: Ocean Science , Special Feature: The Multidisciplinary Drifting Observatory for the Study of Arctic Climate (MOSAiC)

Benjamin Rabe, Céline Heuzé, Julia Regnery, Yevgeny Aksenov, Jacob Allerholt, Marylou Athanase, Youcheng Bai, Chris Basque, Dorothea Bauch, Till M. Baumann, Dake Chen, Sylvia T. Cole, Lisa Craw, Andrew Davies, Ellen Damm, Klaus Dethloff, Dmitry V. Divine, Francesca Doglioni, Falk Ebert, Ying-Chih Fang, Ilker Fer, Allison A. Fong, Rolf Gradinger, Mats A. Granskog, Rainer Graupner, Christian Haas, Hailun He, Yan He, Mario Hoppmann, Markus Janout, David Kadko, Torsten Kanzow, Salar Karam, Yusuke Kawaguchi, Zoe Koenig, Bin Kong, Richard A. Krishfield, Thomas Krumpen, David Kuhlmey, Ivan Kuznetsov, Musheng Lan, Georgi Laukert, Ruibo Lei, Tao Li, Sinhué Torres-Valdés, Lina Lin, Long Lin, Hailong Liu, Na Liu, Brice Loose, Xiaobing Ma, Rosalie McKay, Maria Mallet, Robbie D. C. Mallett, Wieslaw Maslowski, Christian Mertens, Volker Mohrholz, Morven Muilwijk, Marcel Nicolaus, Jeffrey K. O'Brien, Donald Perovich, Jian Ren, Markus Rex, Natalia Ribeiro, Annette Rinke, Janin Schaffer, Ingo Schuffenhauer, Kirstin Schulz, Matthew D. Shupe, William Shaw, Vladimir Sokolov, Anja Sommerfeld, Gunnar Spreen, Timothy Stanton, Mark Stephens, Jie Su, Natalia Sukhikh, Arild Sundfjord, Karolin Thomisch, Sandra Tippenhauer, John M. Toole, Myriel Vredenborg, Maren Walter, Hangzhou Wang, Lei Wang, Yuntao Wang, Manfred Wendisch, Jinping Zhao, Meng Zhou, Jialiang Zhu

* Email: benjamin.rabe@awi.de
* Email: celine.heuze@gu.se

Elementa: Science of the Anthropocene (2022) 10 (1): 00062.
https://doi.org/10.1525/elementa.2021.00062 Article history

Arctic Ocean properties and processes are highly relevant to the regional and global coupled climate system, yet still scarcely observed, especially in winter. Team OCEAN conducted a full year of physical oceanography observations as part of the Multidisciplinary drifting Observatory for the Study of the Arctic Climate (MOSAiC), a drift with the Arctic sea ice from October 2019 to September 2020. An international team designed and implemented the program to characterize the Arctic Ocean system in unprecedented detail, from the seafloor to the air-sea ice-ocean interface, from sub-mesoscales to pan-Arctic. The oceanographic measurements were coordinated with the other teams to explore the ocean physics and linkages to the climate and ecosystem. This paper introduces the major components of the physical oceanography program and complements the other team overviews of the MOSAiC observational program. Team OCEAN's sampling strategy was designed around hydrographic ship-, ice- and autonomous platform-based measurements to improve the understanding of regional circulation and mixing processes. Measurements were carried out both routinely, with a regular schedule, and in response to storms or opening leads. Here we present along-drift time series of hydrographic properties, allowing insights into the seasonal and regional evolution of the water column from winter in the Laptev Sea to early summer in Fram Strait: freshening of the surface, deepening of the mixed layer, increase in temperature and salinity of the Atlantic Water. We also highlight the presence of Canada Basin deep water intrusions and a surface meltwater layer in leads. MOSAiC most likely was the most comprehensive program ever conducted over

the ice-covered Arctic Ocean. While data analysis and interpretation are ongoing, the acquired datasets will support a wide range of physical oceanography and multi-disciplinary research. They will provide a significant foundation for assessing and advancing modeling capabilities in the Arctic Ocean.

Keywords: Physical oceanography , MOSAiC, Arctic, Coupled, Drift, Sea ice

Topics
Ocean Science , The Multidisciplinary Drifting Observatory for the Study of Arctic Climate (MOSAiC) .

1. Introduction

The Arctic is critical for the global climate system and is reacting fastest to current climate change. The Arctic is warming more than twice as fast as the global average (Ballinger et al., 2020 ; Thoman et al., 2020), and the sea-ice cover is dramatically receding (IPCC, 2013 ; Meredith et al., 2019). Various linkages between the Arctic and lower latitudes (e.g., Somavilla et al., 2013 ; Florindo-Lopez et al., 2020) highlight the connection to the global oceans, although models and observations diverge on the nature of these linkages (Cohen et al., 2020). The Arctic intermediate and deep waters, in particular, are part of the global ocean conveyor belt, significantly contributing to the overflow in the Denmark Strait and the formation of North Atlantic Deep Water (Rudels, 2009). Yet, compared to the remainder of the world oceans, relatively few and seasonally limited observations have been made in the Arctic Ocean: fewer than 700 full-depth temperature/salinity profiles existed in the whole deep Arctic north of 82°N prior to 2019, according to publicly available data collections (e.g., UDASH, Behrendt et al., 2018 ; World Ocean Database, 2018, Boyer et al., 2018), and only 40 of those were obtained during winter. That is about half the total number in Fram Strait alone, and significantly less than in the North Atlantic. These limited observations are often too far apart in both space and time for process- and climate-relevant studies. Quasi-synoptic coverage of the near-surface layers in the Arctic Ocean is practically impossible due to the small covariance scales in space and time (e.g., Sumata et al., 2018). Observational climatology and high-resolution ocean model output have shown that some of the observed eddies in the Arctic are of a size comparable to the first mode baroclinic Rossby radius, whereas others are closer to the second mode (Nurser and Bacon, 2014). Sub-mesoscale features are reported to occur on scales as small as 1 km (Timmermans et al., 2012). Hence, we primarily rely on local process studies and upscaling using other data products, such as reanalysis.

This lack of spatially and temporally adequate observation is largely due to the logistical difficulties of accessing the ice-covered central Arctic Ocean, in particular outside the summer. Many Arctic observation programs (e.g., Polyakov et al., 2013 ; Rabe et al., 2014 ; Behrendt et al., 2018 ; Proshutinsky et al., 2019) are based on icebreaker surveys that often suffer from time constraints on station time, not allowing comprehensive measurements over a full tidal, inertial or diurnal cycle, or the duration of short-term events such as passing storms, although targeted airborne campaigns can fill part of thesseasonal gap, e.g., the North Pole Environmental Observatory (NPEO; Morison et al., 2002). Furthermore, sustained in-situ measurements at high temporal resolution, such as profiling of microstructure turbulence, are personnel intensive and require complex logistics. Several Arctic drift expeditions have, hence, been carried out to investigate the seasonal cycle of upper ocean properties and interaction with the whole climate system.

After Nansen's pioneering drift across the Arctic Ocean (Nansen, 1902), sea-ice and glacier fragments or "ice islands" served as the basis for year-round Russian drifting ice camps (North Pole-1 to 40; Shirshov and Fedorov, 1938 ; Frolov et al., 2005). In the North American Arctic, the Arctic Ice Dynamics Joint Experiment (AIDJEX), resulted in an improved sea-ice model that considered feedback from ocean and atmosphere (e.g., Untersteiner et al., 2009). Other campaigns have focused specifically on ocean internal waves and turbulent mixing, such as the Arctic Internal Wave Experiment (AIWEX; e.g., Levine, 1990). The Surface Heat Budget of the Arctic Ocean (SHEBA) drift with CCGI *Des Groseilliers* quantified the surface energy budget between the snow-covered sea ice and the cloudy atmosphere, in addition to a comprehensive upper ocean program, in the then thick and consolidated ice cover of the Canada Basin from October 1997 to October 1998 (Perovich et al., 1999 ; Perovich and Moritz, 2002 ; Krishfield et al., 2005). The sailing vessel *Tara* drifted with the ice in the Transpolar Drift for about 2 years in 2006–2008, though physical ocean observations were limited (Pesant et al., 2015). Recently the N-ICE2015 drift carried out multidisciplinary observations from RV *Lance* in rather thin sea ice north of Svalbard in January–June 2015. The expedition highlighted, in particular, the response of the ocean to storm events (Granskog et al., 2018 ; Graham et al., 2019). To date, manual surveys using icebreakers or drifting ice camps are the only means for extensive water sampling, including chemical provenance tracers (e.g., Bauch et al., 2011 ; Laukert et al., 2017a , 2019) to analyze large-scale circulation and water mass transformation (e.g., Laukert et al., 2017b), as well as the pathways of Siberian river runoff (Laukert et al., 2017c; Paffrath et al., 2021).

In addition to in-situ observations requiring personnel, autonomous ice-tethered drifting ocean observing platforms have become increasingly important for observing the Arctic Ocean region during the past three decades (Toole et al., 2006 ; Kikuchi et al., 2007 ; Hatakeyama et al., 2001 ; Stanton et al., 2012 ; Koenig et al., 2016 ; Athanase et al., 2019). These types of instrument systems usually rely exclusively on electronic sensors and are typically limited to the top 1000 m of the Arctic Ocean. Though providing year-round time series, they are mostly aimed at large-scale monitoring, and often instrumentation on the same ice floe do not encompass the whole coupled system. Exceptions include the Marginal Ice Zone program in the Canada Basin (Lee et al., 2017). Other autonomous in-situ observations are seafloor moorings. Although they have been operated under the sea ice as far north as the north pole for a whole decade (Aagaard and Johnson, 2011), they are difficult to deploy and recover under perennial ice cover, often requiring divers or remotely operated vehicles. In addition, shallow components are threatened by the ridge keels in drifting sea ice. Therefore, operating a series of complex moorings to capture the ocean-ice-atmosphere system is particularly challenging in the Eurasian central Arctic Ocean; successful examples are the Nansen and Amundsen Basin Observing System (NABOS; e.g., Polyakov et al., 2012) and the NPEO (Aagard and Johnson, 2011). Finally, dedicated satellite missions provide an opportunity for observations not requiring in-situ field logistics. Already today they can provide important Arctic-wide information about the ocean state, including sea surface height, dynamic topography and geostrophic surface currents (Armitage et al., 2016 , 2017), as well as sea surface temperature (Steele and Dickinson, 2016) and wave height (Stopa et al., 2016). However, observing ocean currents from space directly is limited to regions that are ice-free, at least seasonally, and observations at the mesoscale and sub-mesoscale are additionally hampered by comparatively coarse spatial or temporal resolution. These limitations are being resolved

only slowly by missions in preparation (e.g., Kilic et al., 2018) or proposed (Commenginger et al., 2019; Lopez-Dekker et al., 2019). The Multidisciplinary drifting Observatory for the Study of the Arctic Climate Climate (MOSAiC) program as a whole, and the physical oceanography component in particular, have thus been designed to make use of all of the advantages of these different methods: a ship- and ice-based drifting platform augmented by distributed autonomous instrumentation (additional article expected in this special collection, led by B Rabe), with multiple measurements over an inertial time period, including water mass analysis and various chemical tracers, coordinated with high-resolution runs of regionally focused ice-ocean general circulation models and satellite observations.

The MOSAiC program strived to provide complete, holistic observations of the Arctic physical oceanography and coupled seasonal processes (Figure 1). As the Arctic perennial sea-ice cover becomes increasingly seasonal (Haine and Martin, 2017; Perovich et al., 2020), larger ocean areas are now directly exposed to the atmosphere for at least part of the year. As a result, the exchange of heat, moisture and momentum between the ocean and atmosphere has intensified (Martin et al., 2016; Timmermans et al., 2018; Ivanov et al., 2019). In addition, boundary transports have changed, such as increasing continental runoff and the inflow of waters of Atlantic and Pacific origins (e.g., Polyakov et al., 2011; Woodgate, 2018). As a result of external forcing and regional processes within the Arctic Ocean, regional changes in circulation and stratification have been observed (Li et al., 2020), notably the Atlantification of the Eurasian Arctic basin (Polyakov et al., 2017, 2020). These changes have impacted large-scale ocean circulation (Rudels et al., 2015; Armitage et al., 2016), water mass distribution (Rudels et al., 2013; Timmermans and Jayne, 2016; Timmermans and Marshall, 2020), upper ocean freshwater content (Rabe et al., 2011; Korhonen et al., 2013; Rabe et al., 2014; Haine et al., 2015; Solomon et al., 2021), shelf-slope cascading into the deep (Luneva et al., 2020), small-scale to mesoscale processes (Fer, 2014; von Appen et al., 2018), supply of nutrients to the photic zone (Nishino et al., 2011; Yamamoto-Kawai et al., 2011; Torres Valdes et al., 2016) and productivity of the marine ecosystem (Arrigo and van Dijken, 2011; Lowry et al., 2018). Another example is the potential impact of the interruption of ice transport from the Siberian Shelf seas to the central Eurasian Arctic Ocean and Fram Strait (Krumpen et al., 2019). The influence of these changes on the hydrography, biogeochemistry and ecosystem within and outside the freshwater-rich Transpolar Drift (Paffrath et al., 2021) remains to be investigated.

Figure 1.

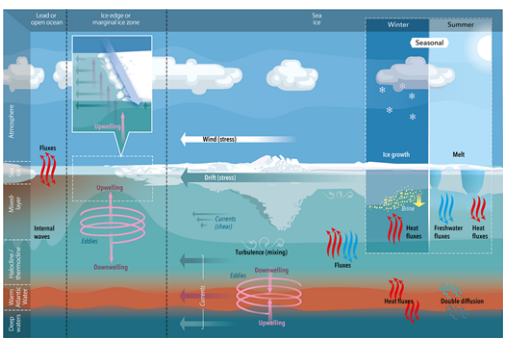

View large Download slide

Oceanographic processes studied in Multidisciplinary drifting Observatory for

the Study of the Arctic Climate (MOSAiC) . Schematic representation of physical oceanography processes relevant to Team OCEAN during the MOSAiC expedition. The vertical extent of the under-ice boundary layer has been exaggerated; the left-hand column showing air-sea fluxes and internal waves represents either a lead, bounded by sea ice, or the open ocean beyond the marginal ice zone. DOI: https://doi.org/10.1525/elementa.2021.00062.f1

Moreover, mesoscale and sub-mesoscale currents, surface drag by wind and ice motion, and breaking internal waves result in small-scale turbulence. The Arctic Ocean is often assumed to be a quiescent environment, as internal wave energy tends to be low under the Arctic Ocean ice cover (Levine et al., 1985) and background mixing rates have been reported close to molecular levels (e.g., Fer, 2009). However, post-storm conditions can lead to enhanced mixing (McPhee et al., 2005 ; Fer, 2014 ; Meyer et al., 2017), the role of which in the upper central Arctic Ocean is still not well known. Furthermore, mesoscale and sub-mesoscale variability facilitate intense vertical motion in the polar regions (Lévy et al., 2012 , 2018 ; Biddle and Swart, 2020), while turbulence enhances vertical fluxes relative to background molecular diffusion; together, they modulate the upper ocean heat and salt/freshwater budgets, biogeochemical substances such as nutrients and carbon compounds, and sea-ice variability. In the changing ice-free Arctic, we expect an increased input of wind energy (Lehner et al., 2012 ; Kawaguchi et al., 2015). However, the fraction of energy penetrating into the water column and its contribution to mixing are uncertain (Alford et al., 2016 ; Guthrie and Morison, 2021), leading to uncertainty in estimates of vertical fluxes of oceanic heat, salt, momentum, nutrients and dissolved gases. Hence, making routine observations of mixing as the MOSAiC observatory drifted and targeted observations during storm conditions were objectives of the observational program.

Besides comprehensive and novel observations, the main objective of MOSAiC is the ultimate improvement of climate models. Global climate models are heavily biased in the Arctic Ocean, in particular because of their incorrect representation of vertical mixing processes. This caveat results in large biases in ocean temperature and salinity (Ilicak et al., 2016) and prevents progress in quantifying their effects on large-scale circulation (Timmermans and Marshall, 2020). In addition to relying on mixing parameterizations, many of these models have a resolution in the horizontal and vertical too coarse to resolve mesoscale and smaller-scale processes. Observations to improve or tune them are still too limited, spatially and temporally, and, in particular, do not resolve interannual variability (e.g., Behrendt et al., 2018); even fewer observations of turbulent mixing are available (e.g., Fer, 2009 ; Meyer et al., 2017).

Given the state of knowledge and observations of the Arctic Ocean, the physical oceanography program during MOSAiC aimed to answer the following questions (summarized in Figure 1):

- What is the temporal change in water masses and heat content of the deep Eurasian Basin? Where do these water masses originate, and how does their distribution relate to current knowledge of shelf-basin exchange?
- How are vertical fluxes of heat and mass (salt, nutrients, dissolved gases) between the warm Atlantic Water layer, the halocline, and the mixed layer governed in the ice-covered Arctic interior, and how does that contrast with the marginal ice zone? What are their seasonal cycles?
- How do these vertical fluxes fit in the entire coupled system? What is the impact of changing atmospheric conditions on them? What is the role of

small-scale variability in the under-ice boundary layer? What about ice topography, such as ridges? How do the processes associated with these questions affect the biogeochemistry and the ecosystem?

The MOSAiC fieldwork was carried out during a drift expedition with the research icebreaker *Polarstern* (Alfred-Wegener-Institut Helmholtz-Zentrum für Polar- und Meeresforschung, 2017) from October 2019 through September 2020, in the Eurasian Basin and Fram Strait (see Figure 2), and encompassed an unprecedented set of multidisciplinary measurements over a full annual cycle. There were five field teams named Atmosphere (ATMOS; Shupe et al., 2022), Sea Ice (ICE; Nicolaus et al., 2022), Biogeochemistry (BGC; overview article anticipated for this special collection, led by E Damm), Ecology (ECO; overview article anticipated for this special collection, led by AA Fong), and Physical Oceanography (OCEAN; this manuscript). Throughout this manuscript, we will use the name Team OCEAN to refer to the latter team. The expedition consisted of five legs and three drift periods: Legs 1–3 (October 2019 to early June 2020); Leg 4 (June to late July 2020) at the same floe as the first drift; and Leg 5 (August–September 2020) at a second floe. At the end of Leg 3, *Polarstern* was forced to transit to Svalbard and back for personnel exchange complicated by COVID-19 travel restrictions, then returned to the same floe that was used by Leg 3 for Leg 4 (see map in Figure 2; the floe drifted about 1° southward from 83.4°N without *Polarstern*, from May 16 to June 19). At the end of Leg 4, in late July, the ice floe disintegrated. Therefore, the drift during Leg 5, from mid-August, took place on a different floe, after *Polarstern* relocated to the Eurasian central Arctic Ocean, around the same region as Leg 2 had passed near the North Pole about half a year before. The expedition encountered different ice conditions, from the marginal ice zone to consolidated ice cover. The overall approach of this study of the coupled climate system in the Eurasian Basin of the Arctic Ocean is described in the MOSAiC general overview, along with further overall logistical information (additional overview article expected in this special collection, led by M Rex). All observations considered the effect of the physical system on the ecosystem, biogeochemical processes and dissolved gases. The related quantities and processes are illustrated in Figure 1.

Figure 2.

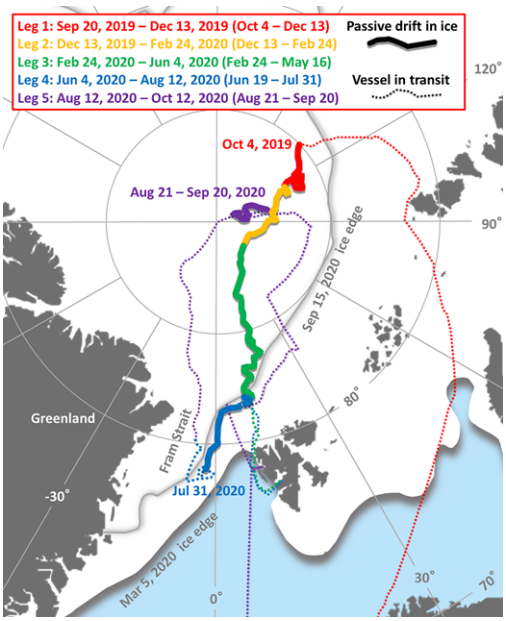

View large Download slide

Main dates and location of the Multidisciplinary drifting Observatory for the Study of the Arctic Climate (MOSAiC) expedition . Track of the 5 different legs of the MOSAiC expedition while Polarstern was drifting with the sea ice (solid lines, dates given; dates excluding transit in parentheses) and in transit (dashed lines) during arrival and exchange (see inset legend). After Shupe et al. (2020) . DOI: https://doi.org/10.1525/elementa.2021.00062.f2

The physical oceanography work conducted during the MOSAiC drift focused on:

- monitoring the full water column in the Transpolar Drift in the Eurasian Basin of the Arctic Ocean over a full annual cycle. In the upper ocean the observations provide information on seasonal and regional variability, whereas in the deep ocean they provide an assessment of the quasi-synoptic state;
- resolving vertical ocean processes as part of the coupled ice-ocean-atmosphere system in regional and global climate; and
- assessing three-dimensional variability at the mesoscale and sub-mesoscale, in particular in response to events such as storms and opening leads.

This manuscript presents an overview of the physical oceanography work within MOSAiC to date. Section 2 outlines the observational approach and schematic implementation of our year-round observations along the MOSAiC drift. Section 3 describes the instrumentation and setup used to obtain the measurements; more details can be found in Text S1. The resulting observational datasets are outlined in Section 4, and preliminary results are shown in Section 5. Section 6 highlights the linkages between physical oceanography observations and results to remote sensing, numerical modeling, and the work of the other field teams, before concluding in the context of the coupled system in Section 7.

2. Overview of the Team OCEAN observational program

To fill the gaps in our knowledge of the different processes and variables outlined in Section 1 and Figure 1, the MOSAiC Team OCEAN observational program covered different spatial and temporal scales, from right under the ice to just above the seafloor. Numerous observations within the ocean, in the ice and snow, and in the atmosphere were further coordinated with the other teams to capture the instantaneous state of the local atmosphere-ice-ocean column. Our manual observations were carried out largely from the central observatory (additional article expected in this special collection, led by M Nicolaus), an area encompassing *Polarstern* and its immediate surroundings on the ice floe (Figures 3 and 4; Section 3):

- The *Polarstern* was used to operate heavy equipment throughout the entire water column. The main system was lowered from *Polarstern* through an ice hole (*Polarstern* -hydrohole) to measure hydrographic properties and sample large volumes of water.
- Ocean City, located approximately 300 m away from *Polarstern* , was used for upper ocean observations away from the influence of *Polarstern* in a logistically equipped environment. During the cold and partially dark part of the drift, we operated from a tent with a base area of 18 m^2 (Figure 3). A thick, buoyant floor and insulated tent structure, electricity and heating provided a sheltered working environment. Fixed-depth and profiling sensor packages were lowered there through an ice hole in

the floor (Ocean City-hydrohole). In addition, the tent was connected to the *Polarstern* computer network for easy exchange of data. During Legs 1–3, Ocean City functioned as a partial backup for the *Polarstern* - hydrohole. The fixed installation was replaced with an uncovered solid base around the Ocean City-hydrohole or a mobile tent during the final two legs. The various implementations are illustrated in Figure 5, and reflect the changing environmental conditions and logistical constraints throughout the drift.

Figure 3.

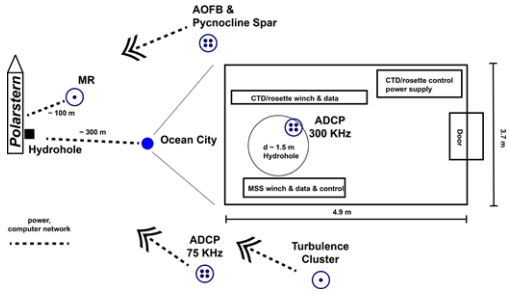

View large Download slide

Schematic representation of the physical oceanography installations . Installations near *Polarstern*, zoom-in on Ocean City, and location of instruments on the ice. Several other sites and installations were run by other Multidisciplinary drifting Observatory for the Study of the Arctic Climate teams within about 2 km from *Polarstern* (see Figure 4). The dashed lines/arrows denote a power and data link to the ship. For details on the installed devices, see Section 3. DOI: https://doi.org/10.1525/elementa.2021.00062.f3

Figure 4.

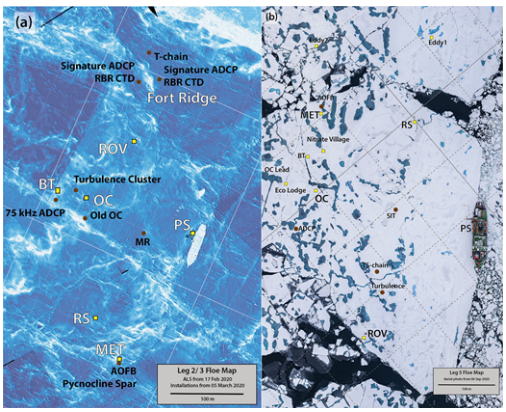

View large Download slide

The central observatory throughout Multidisciplinary drifting Observatory for the Study of the Arctic Climate . Distribution of central observatory sites and measurements with focus on the physical oceanography installations at the beginning of (a) Leg 3 on March 5, 2020 and (b) Leg 5 on September 6, 2020. Main central observatory sites are marked by yellow squares and white labels: *Polarstern* - hydrohole, the Ocean City (OC) tent and hydrohole, the location of OC prior to the large shear event during Leg 1 (old OC), remote sensing, balloon town, remotely operated vehicle, met city, ridge observatory Legs 2–3 (fort ridge), salinity ice tether, and ridge observatory Leg 5 (Eddy 1 and Eddy 2). Details on installed devices (black labels) can be found in Section 3. The background in (a) reflects ice elevation, where white is elevated and dark blue is thin/level ice. The image is preliminary from airborne laser scanner surveys from February 17, 2020 and represents the ice conditions on March 5; it is shown only as a rough indication of the ice surface (the finally processed data set will be made available publicly in the near future). The background in (b) is an aerial photograph from September 6, 2020 (photo credit: Marcel Nicolaus). Further details of the evolution of the observatory and a wider view

will be available in the overview of the Central Observatory (article anticipated for this special collection, led by M Nicolaus). DOI: https://doi.org/10.1525/elementa.2021.00062.f4

Figure 5.

View large Download slide

Ocean City at different stages of Multidisciplinary drifting Observatory for the Study of the Arctic Climate . Pictures showing the tent with buoyant and reinforced floor (a) during Legs 1–3 from inside, (b) during Legs 1–2 from outside during polar night, and (c) during Leg 3 from outside with mobile power supply. Leg 4 used the remotely operated vehicle hole of Team ICE for part of the operations (d), similar to the Ocean City-hydrohole, without further shelter (not shown), whereas during Leg 5 a mobile tent (view outside, (e) allowed measuring in a protected environment inside (f). Photo credits are Ying-Chih Fang (a and b), Janin Schaffer (c), Morven Muilwijk (d), and Mario Hoppmann (e and f). DOI: https://doi.org/10.1525/elementa.2021.00062.f5

The Ocean City measurements were supplemented by partly or fully autonomous devices at other sites in the Central Observatory, as given in Figure 3, and by a Distributed Network of autonomous ice-tethered systems ("buoys") in a radius of approximately 40 km around the Central Observatory. This strategy allowed to estimate the representativeness of the observations carried out in the Central Observatory, to resolve synoptic mesoscale variability, and detail quasi-synoptic sub-mesoscale features by rapid measurements along the drift track. Part of the Distributed Network was comprised of three sites, within about 25 km from the Central Observatory, with complex systems to obtain profile measurements of ocean temperature, salinity, oxygen and bio-optical variables from the surface to the intermediate Atlantic Water, as well as ocean flux measurements under the ice and in the halocline.

A further eight sites with lighter equipment for ocean observations, within about 40 km, comprised devices for shallower profiling and fixed-depth measurements of temperature and salinity with high temporal resolution. The Distributed Network was overall made up of instruments from multiple disciplines, including observations of snow, ice and atmosphere. The layout and different measurement systems will be described in a summary (article expected in this special collection, led by B Rabe).

During the expedition, the distribution of physical oceanography installations in the Central Observatory changed. The original setup in the marginal ice zone around 85°N in the eastern Amundsen Basin led to installations arranged roughly along a line on the starboard side of *Polarstern*, with the cables supplying power and computer network connecting the different sites to *Polarstern*. The location of Ocean City was

determined after surveying areas of level ice ranging from 0.6 to 1.2 m in thickness in an approximately 50 x 50 m^2 area, and a minimal distance of 30 m from ridged ice. In the middle of Leg 1 (late November 2019), the floe suffered a major fault and shear deformation, displacing several of the sites along a line roughly 100 m from the bow of *Polarstern* (Figure 4a). This event led to strong ridging that forced Ocean City to be moved to a location about 50 m from the new ridge, which was up to several meters tall (clearly visible as a white line on Figure 4a). Ice conditions in the Central Observatory remained fairly stable until the middle of Leg 3 (mid-March 2020), when large cracks and leads formed across the floe, separating several of the sites and cutting directly underneath *Polarstern*. However, the relative locations of *Polarstern* and the sites Ocean City and Remotely Operated Vehicle (ROV in Figure 4a) of Team ICE did not change. Due to various external factors, primarily the COVID-19 pandemic, *Polarstern* had to leave the floe after Leg 3 to exchange supplies and personnel near Svalbard. After return to the same floe during Leg 4 the *Polarstern* anchored to a different location along the floe, and the Ocean City site was set up about 1 km from its location toward the end of Leg 3. The Central Observatory ended in the central Fram Strait at the end of Leg 4. A new Central Observatory was set up on a different floe in the Eurasian central Arctic Ocean during Leg 5 (Figure 4b).

Throughout the MOSAiC expedition, routine upper ocean profile measurements at the Central Observatory formed an important component of the experiment. Our field program focused on observing a comprehensive set of variables (described in detail in Sections 3 and 4) at the Central Observatory, measured once a week, several times each day, or continuously. In addition to covering most of the annual cycle, this wide range of physical ocean observations, coordinated with biogeochemical and ecological water samples taken by other teams, formed the main added value of Central Observatory observations. Further, concurrent observations of the ice, the snow and the atmosphere aimed to close the full column budget in terms of momentum, heat and mass fluxes.

Our strategy included weekly full-depth hydrographic casts from *Polarstern* to capture the state of the full water column for a variety of variables, thereby resolving regional and seasonal variability. This effort included high-resolution sampling for tracers and biogeochemical variables. Sampling was coordinated across Teams OCEAN, ECO, and BGC, with specific aspects of sampling detailed in each team overview (Sections 3 and 4; additional overview articles expected in this special collection, led by E Damm and AA Fong). Casts down to a few hundred meters depth collected from Ocean City several times each week allowed identifying the effect of varying surface conditions along the drift track, which include ice drift, storms, fronts and eddies. The full set of hydrographic casts further allow us to derive large-scale advection, in particular when complemented with tracers. The casts were complemented by sets of profiles of microstructure turbulence to estimate vertical mixing and associated heat and mass fluxes. These measurements allow us to resolve sub-daily variability in water column stratification, for example, due to internal waves, mesoscale eddies or sub-mesoscale filaments. In addition to regular observations, we carried out event-driven measurements: at the regular sites with higher time resolution, e.g., during storms; and at temporary sites, e.g., in newly formed leads. The various projects that contributed to MOSAiC planning and Team OCEAN fieldwork are listed in Table S1.

3. Instruments and methods

We used a multitude of instruments and sensor packages within the infrastructure and observational approach outlined in Section 2. The remainder of this section briefly describes the use of those methods and instruments (in bold font, linking abbreviations to figures), either under responsibility of Team OCEAN or with their significant involvement. Further detail can be found in Text S1. The resulting datasets and operational challenges are described in Section 4.

3.1. Primary profiling CTD operations

Conductivity-temperature profiling through depth (CTD) provides the basis for physical oceanography programs. In general, the CTD unit is lowered through the water column while measuring conductivity, temperature and pressure, resulting in vertical resolution of 1 m or finer in the final depth-gridded salinity and temperature profiles. During MOSAiC, we used four different systems: a full-depth CTD operated from the *Polarstern*; a 1000-m depth CTD operated from the ice; 1000-m depth expendable CTDs (XTCD) used during transit; and a 600-m depth stand-alone CTD, usually mounted on a fishing-rod for mobile measurements. The microstructure profilers also included a CTD sensor package (see Section 3c for details). Note that Teams ICE, ECO and BGC had additional CTDs on some of their instruments for specific purposes; the reader is invited to check their respective overview publications for more information (Nicolaus et al., 2022; additional overview articles expected in this special collection, led by E Damm and AA Fong).

For most of the year of MOSAiC, we had two CTD/rosette systems in operation: one 24-bottle CTD/rosette from *Polarstern* (PS-CTD; Figures 6a and 7) and one 12-bottle CTD/rosette from Ocean City during Legs 1–3 (OC-CTD; Figures 6b and 7). The PS-CTD used Ocean Test Equipment bottles, operated on a *Polarstern* wire, and was able to sample the full water column. The OC-CTD used Niskin bottles, was operated on a mobile winch system, and could only reach a maximum depth of about 1170 m. As Ocean City was about 300 m away from *Polarstern* (Figure 3; additional article expected in this special collection, led by M Nicolaus), the OC-CTD allowed observation of the upper water column without potential disturbance by *Polarstern* that may have occurred for the PS-CTD. Both the PS- and OC-CTD were configured in the standard SeaBird SBE911plus setup, equipped with pumped duplicate sensors for temperature, conductivity, and dissolved oxygen, along with single sensors for pressure, fluorescence (chlorophyll *a* and chromophoric dissolved organic matter, CDOM), photosynthetically active radiation (PAR), and beam transmission. As only one CDOM sensor was available, the sensor was swapped in-between CTDs from time to time. An altimeter was mounted on the PS-CTD to monitor the distance to the seafloor. Furthermore, two internally recording sensor packages were attached to the CTD frame: an Underwater Vision Profiler (UVP) and a Satlantic Submersible Ultraviolet Nitrate Analyzer (SUNA), the latter only connected for profiles shallower than 2000 m. The former was battery-powered while the latter received power only from the SBE911plus. During Legs 3, 4 and 5, a surface reference measurement of photosynthetically active radiation (SPAR) was installed on the ice (Leg 3) or on *Polarstern* (Legs 4–5) to measure radiation during a CTD cast. Additionally, during Legs 4–5, a second SPAR sensor, right next to the first one, was operated continuously with a separate data logger. A methane (CH_4) sensor was mounted on the OC-CTD during Legs 1–3. A rhodamine sensor was mounted from Leg 4, though flooded during Leg 5; further details can be found in Nicolaus et al. (2022). The accuracy of the preliminary temperature data is better than ± 0.01 °C, and of the salinity

data is better than ± 0.01 g kg $^{-1}$. To prevent freezing damage during Arctic winter conditions, a heated shelter was developed to isolate the PS-CTD from the frigid air (red shelter on top of CTD/rosette in Figure 6a), and further adjustments to the usual CTD/rosette operation were made. Details are given in Text S1.

Figure 6.

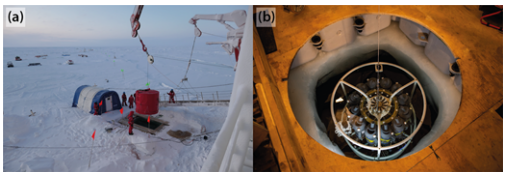

View large Download slide

Selected images of installations during operation . Conductivity-temperature profiling through depth (CTD)/rosette with red shelter during operation at the *Polarstern*-hydrohole and the tent used to protect the hydrohole outside hours of operation (a); CTD/rosette in Ocean City during deployment in the hydrohole (b). Photo credits are Janin Schaffer (a) and Esther Horvath (b). DOI: https://doi.org/10.1525/elementa.2021.00062.f6

Figure 7.

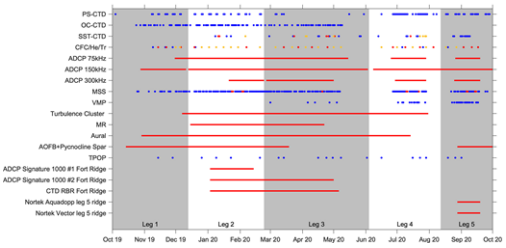

View large Download slide

Time line of successful measurement of Team OCEAN instrument systems . Dots denote days where one or more profiles were carried out. The solid lines denote continuous time-series measurements. Interruptions shorter than 1 day are not shown. The different colors indicate different types of sampling. The abbreviations for the different measurement systems are given in Section 3 (bold font). For SST-CTD profiles, blue indicates regular profiles, red indicates distributed network/buoy cross-calibration, and orange indicates PS-/OC-CTD or MSS calibration. For CFC/He/Tr, blue indicates CFC + SF6, red indicates CFC + SF6 + He + Ne, and orange indicates CFC + SF6 + He + Ne + Tritium. For MSS, blue indicates minimum measurements (n = 3 or more) and red indicates intensive measurements (12 h or more). The temporary temperature and salinity chain deployments are not shown. SST = Sea and Sun Technologies; CTD = conductivity-temperature profiling through depth; PS = Polarstern-hydrohole; OC = Ocean City; MSS = microstructure sonde. DOI: https://doi.org/10.1525/elementa.2021.00062.f7

A stand-alone CTD, the SST 48 M CTD (SST-CTD ; Sea and Sun Technologies, Germany; Figure 7), was used to obtain additional measurements in the field with a set of unpumped sensors for conductivity, temperature and pressure. The SST-CTD is a self-contained, battery-powered instrument package that was used with a battery-powered fishing rod. Profiles down to 600 m were obtained with this mobile system that easily fit into a helicopter or onto a small sledge. We further used the SST-CTD attached to a line close to messenger-triggered water sampling bottles to obtain sensor data at the time of sampling. The system was used, in particular, for cross-calibration of autonomous ocean buoys of the Distributed Network (Legs 2–4), during lead-opening events (Legs 2–5), for collecting temperature/salinity profiles above the Yermak Plateau (Legs 3 and 4), in combination with turbulence measurements in leads (Leg 4), with team ECO during a diurnal sampling

campaign (Leg 4), to complement the PS-CTD when it was not running because the *Polarstern* -hydrohole could not be used (Leg 3), and to measure the hydrographic properties of the freshwater lens (Legs 4 and 5).

An expendable CTD system was used to obtain CTD profiles down to 1100-m depth while underway, from *Polarstern* and from the sea ice. The XCTDs were deployed in transit to the Eurasian central Arctic Ocean during Leg 5 while breaking ice or transiting a polynya.

3.2. Water sampling

The bottles on the PS- and OC-CTD allow for collection of water at discrete depths, fired during the upcast. The water was collected by members of the teams OCEAN, BGC and ECO. The sampling order followed the GO-SHIP protocol (Sloyan et al., 2019). Salinity samples were collected first from dedicated bottles that were not used for tracer gas sampling. The tracer and gas samples are used to study vertical exchange and horizontally advected water mass signatures.

We collected and analyzed onboard salinity samples during the weekly PS-CTD casts, for calibration of the CTD sensors by correcting the conductivity. Samples were analysed onboard, and the results will contribute to the finally processed datasets of the OC-CTD and the PS-CTD.

Trace gases that do not interact biogeochemically in the ocean are valuable tools to study physical processes and ocean circulation. During MOSAiC, we sampled transient tracers of anthropogenic origin (see also Figure 7): chlorofluorocarbons (CFCs), sulfur hexafluoride (SF_6), tritium (^3H), and the noble gases and their isotopes: helium (He) and neon (Ne). During weekly PS-CTD casts, transient tracer samples were collected over 12 depths covering the entire water column. These samples were the first to be collected at the rosette, with noble gases collected only for the top 500 m. Noble gas and transient tracer samples were stored onboard until the end of the expedition for later analysis on land.

For tracer-based provenance studies, water samples for the concentration of oxygen and hydrogen isotopes ($\delta^{18}O$ and δD), as well as neodymium (Nd) isotopes and rare earth elements (REE) were taken in cooperation with the BGC team. Samples for $\delta^{18}O$ and δD were taken from the upper 100 to 300 m one or more times each week. Samples for dissolved radiogenic Nd isotopes and REEs were taken on a monthly basis at four depths (surface, 50 m, 100 m and 200 m). All samples were stored onboard for later analysis on land.

To determine bulk estimates of vertical mixing, beryllium 7 (^7Be) was sampled in the upper water column. ^7Be is a cosmic-ray produced isotope that is deposited upon the ocean surface and subsequently homogenized within the surface mixed layer. The shape of the profile provides a means to determine vertical mixing rates. ^7Be from seawater was sampled within the upper 60 m of the ocean during Legs 2–3. Further details of sampling and analysing this variable will be available in the BGC overview (additional article expected in this special collection, led by E Damm).

3.3. Microstructure profiling

We routinely performed microstructure profiling to quantify high-frequency variability in the water column structure, turbulence and mixing during the MOSAiC drift. Profiling was carried out from the ice using two profilers: a free-falling microstructure sonde (MSS; Figure 7) and an uprising vertical microstructure profiler (VMP; Figure 7). Both devices measure high-resolution vertical profiles of temperature, salinity and shear velocity. The

latter is used to estimate turbulent dissipation rates. The main difference between the two devices is the direction of profiling: the free-falling MSS records data during the descent while the free-rising VMP collects data during the ascent. Some of the MSS profilers we used had additional sensors installed, to measure dissolved oxygen, for example (see Text S1), in the upper ocean down to approximately 350-m depth, leaving a small gap of up to 5 m in turbulent dissipation measurements near the surface. Throughout the expedition, near-daily measurements, including at least 4 profiles and 7 continuous sampling periods were performed, each lasting 12 hours or longer. Ten profiles were also taken in fortuitous lead-opening events. The deployment of the VMP allowed us to record dissipation rates of turbulent kinetic energy in the upper 80 m up to the ice-water interface in order to resolve the under-ice boundary layer and to better quantify the ocean heat fluxes in the upper water column. The instrument was used mainly during Legs 4 and 5, and to a limited extent during Legs 2–3.

3.4. Underway operations

Here we detail the standard underway measurement devices mounted on *R/V Polarstern* with direct relevance to Team OCEAN.

Polarstern is equipped with a shipboard acoustic Doppler current profiler (ADCP) measuring acoustically at 150 kHz to monitor underway ocean currents between water depths of about 15 to 240 m (ADCP 150 kHz ; Figures 3 and 7). This ADCP operated continuously throughout MOSAiC.

The Thermosalinograph system installed on *Polarstern* measures salinity and temperature from a seawater intake at about 11 m depth. During MOSAiC the system was running continuously and only switched off for short maintenance and cleaning. As *Polarstern* was not actively moving for most of the expedition, a pronounced boundary layer may have formed around the *Polarstern* hull in the lee of the drift, one that is not present when the ship speed is higher. Measurements of temperature, in particular, may not be representative of the temperature at the same depth within the region *Polarstern* drifted across. The finally processed data are available in Rex et al. (2021a , 2021b, 2021c), Kanzow et al. (2021) , and Haas et al. (2021) .

3.5. Long deployments of autonomous devices

In addition to manual operation of devices, we deployed several systems in the Central Observatory and on the seafloor to carry out measurements autonomously.

An eddy-correlation ocean flux sensor was deployed on October 14, next to the main meteorology tower (AOFB; Figures 3 , 4a and 7) to measure long time series of ocean momentum, heat and salt fluxes at 3-m depth. In addition, the AOFB measured high-resolution current profiles across the ice-ocean boundary layer into the pycnocline. A primary objective is to compare concurrently the atmosphere-ice-ocean transfer of momentum and heat through the atmosphere-ice and ice-ocean boundary layers over a range of local ice conditions, including during changes in wind direction and storms, and during other influential phenomena.

To study the local vertical turbulent diffusivity and heat fluxes in the pycnocline, a 6-m long pycnocline spar (Figures 3 , 4a, and 7), supporting 24 high-resolution temperature sensors and 3 fast-response thermistors was suspended at 50-m depth adjacent to the AOFB at Met City (Figure 4a). The dataset further allows to study the extreme intermittency of mixing events in terms of the local gradient Richardson number, a measure of the dynamic stability of the water column. Comparison to microstructure

profiling measurements (Section 3c) allows an extended analysis of turbulent mixing events with high temporal resolution.

To obtain velocity observations into the intermediate water layer, a Teledyne RD-Instruments 75 kHz ADCP Longranger (ADCP 75 kHz ; Figures 3 , 4a, and 7) was installed pointing downward under the ice near Site BT (Figure 4a). The installation also included a directional GPS unit with compass as well as data and power links to *Polarstern* . During Leg 4, the installation was self-contained, using batteries and recording internally. The data are available in Baumann et al. (2021) .

To augment the turbulence profiling and increase resolution of velocity in the upper water column, an ADCP measuring at 300 kHz (ADCP 300 kHz ; Figures 3 and 7) was deployed intermittently in the Ocean City-hydrohole at times when the hole was not used for large profiling device; for example, the OC-CTD hydrohole (Legs 2 and 3), and in different hydroholes across the Central Observatory (Legs 4 and 5). The system gathered reliable data of relative horizontal currents and vertical shear in the upper 50 m of the water column, covering most of the upper mixed layer and providing higher vertical resolution than given by the 75 kHz ADCP and the 150 kHz ADCP.

Deployed during Leg 1 and left behind on the floe after Leg 3 to be recovered later, the turbulence cluster mooring consisted of three identical sets of instruments at approximately 25, 45 and 70 m, respectively (turbulence cluster ; Figures 3 , 4a, and 7). The cluster measured velocity, temperature, salinity and partial-pressure CO_2 (pCO_2) around each depth at high temporal resolution between the later part of Leg 1 (December) and Leg 4 (June), though a few instruments stopped measuring from as early as mid-March.

A thermistor chain was installed to measure temperature at high temporal resolution in the top 200 m, with four CTD units at depths of 7, 50, 100 and 200 m to obtain temperature and salinity, and one "microrider" (MR; Figures 3 , 4a, and 7) at 52-m depth to measure temperature microstructure. The MR performed well throughout, from about December until June, but the thermistor chain did not provide data sufficient for further analysis.

In order to record the under-ice soundscape during the MOSAiC drift, an aural autonomous underwater hydroacoustic recorder (Aural) was installed at the second-year-ice (SYI) coring site (also referred to as LM site in the Distributed Network, about 1 km from *Polarstern* during Leg 2) at 50-m depth in late October and was recovered in mid-July 2020. Preliminary screening of the data revealed biophonic, geophonic and anthropophonics contributions to the soundscape.

For studying near-ridge processes, two pairs of ADCP/CTD (ADCP Signature 1000/CTD RBR ; Figures 4a and 7) instruments were deployed at the Leg 2 ridge site (Fort Ridge in Figure 4a) on each flank of the ridge below the ice on January 3, 2020. Nearby deployments from team ICE (thermistor chains for ice-mass balance) and a nearby ocean T-chain and GPS buoys completed the Fort Ridge observatory. During Leg 5, a vector eddy covariance turbulence system (Nortec Vector ; Figure 7) with additional sensors for temperature and dissolved oxygen and an Aquadopp ADCP (Nortek Aquadopp) were deployed just beneath the ice very close to the main ridge on August 28, 2020 (installations marked Eddy 1 and 2 in Figure 4b). Four additional GPS trackers were deployed to determine ridge dynamics, as a complement to the turbulence measurements, in a triangle around the eddy covariance system, at a distance of about 80–90 m.

Tpops are autonomous expendable temperature sensors recording measurements for a fixed time on the seafloor (TPOP; Figure 7). During MOSAiC, 20 units were deployed, on average one every other week just after the full-depth PS-CTD cast. They were configured to take one measurement per hour and to surface on September 1, 2021. As of November 2021, the 5 Tpops deployed during Leg 4 have successfully surfaced and transmitted their data. The other 15, which were deployed further north, are presumed trapped under ice and may send their data in the coming months.

Throughout the expedition we deployed several vertical chains, tethered to the ice, to measure temperature and salinity. These systems contained instruments recording internally, in a surface unit not telemetered or via a fully telemetered buoy. During Leg 2 we deployed one chain covering the upper 60 m, to cover the mixed layer and the upper halocline, at the LM site. During Leg 5 one chain recorded the upper 8-m depth interval at the edge of a newly formed lead. A second chain measured in the upper 100 m (SIT in Figure 4b). A third chain was deployed as a test case in the top 45 m using simple, low-cost conductivity cells (TS-chain in Figure 4b).

A combined nitrate and CTD instrument assembly was used to monitor nitrate, temperature and salinity, either stationary around a depth of 10–20 m or as a manually operated profiler in the upper 100 m. The main purpose was to provide nitrate time series and to supplement the parallel MSS (turbulence) measurements with nitrate data.

An under-ice profiling CTD, the Ice-tethered Profiler (ITP) #111 (ITP111 , Figure 7), was deployed as part of the Distributed Network of autonomous buoys about 15 km from the Central Observatory near the beginning of Leg 1. The instrument system and data processing are described in detail in Toole et al. (2006) , and references therein; the results from this particular ITP are shown in Section 5.

3.6. Data presentation and units

Throughout this work we present our observational data from various CTD sensor packages following the Thermodynamic Equation Of Seawater (TEOS-10; McDougall et al., 2010). TEOS-10 defines absolute salinity, S_A, and conservative temperature, Θ, based on measurements of conductivity, temperature and pressure. All observational data plots have been created either with Ocean Data View (Schlitzer, 2015) or Matlab2021b (Mathworks), including the Gibbs-SeaWater Matlab Toolbox (McDougall and Barker, 2011).

4. Field operation and resulting data sets

The field set up and objectives detailed in Section 2, combined with the instrumentation described in Section 3, led to a weekly schedule of regular observations interspersed with flexible time slots. Team OCEAN was the smallest team, with 3 to 5 people onboard each leg. During a typical week, PS-CTD casts were concentrated on 2 days, due to logistical requirements that included personnel power from many teams and support by the *Polarstern* crew. MSS and OC-CTD profiling were spread across the week to optimize personnel commitment and achieve almost daily time resolution. This effort included coordination with other teams for sampling and operating additional profiling equipment. The MSS operation was constrained by carrying out at least three profiles close in time to allow for statistical averaging when analyzing intermittent turbulence. Blocks of flexible time were allocated to allow for: instrument maintenance, both at the Central Observatory and remotely in the Distributed Network;

preparation of outside fieldwork, such as buoy deployments and event-based additional measurements; preparation of PS- and OC-CTD sampling and operation, e.g., *Polarstern* - and Ocean City-hydrohole maintenance; and data processing and archiving work. The weekly plan varied considerably between legs and seasons, influenced by the size of our team onboard, both seasonal and short-term environmental conditions, continuous measurements during events, and external logistical constraints such as personnel exchange. For example, during Leg 1, the three-person team had to run daily and weekly observations while setting up new installations; likewise, during Leg 3, only three people were onboard keeping the observational program running as strong ice deformation led to the loss of facilities in the Central Observatory. During Legs 2, 4 and 5, more personnel allowed the team to engage in additional measurements, for example, during storm events and for cross-calibration, amid demobilizing and setting up different stages of the Central Observatory.

The MOSAiC observational fieldwork led to an impressive data yield. Despite the pandemic and challenging ice conditions, we obtained nearly year-round records from most of the profiling equipment, CTD/rosette sampling and continuously measuring systems (Figure 7). These include the set of CTD/rosette systems, tracer sampling, current profilers, turbulence cluster and microstructure profilers. The under-ice/halocline flux system (AOFB/Pycnocline Spar) provided good data until the early part of Leg 3. TPOP deployments for deep water measurements covered much of the Eurasian Basin. The SST-CTD was used intermittently, largely for event-targeted measurements and cross-calibration. The ridge devices operated for the duration of the two ridge observatories (Legs 2–3, ADCP Signature 1000 and CTD RBR; Leg 5, Nortek devices).

To ensure optimal data quality we carried out several efforts to facilitate cross-calibration and -comparison between instruments, including mounting the SST-CTD and the MSS profiler on either the PS- or OC-CTD, and carrying out SST-CTD casts at the remote sites in the Distributed Network. Further details will be part of future publications focusing on individual sensors and systems.

Interruptions in our time series were caused by various environmental and operational factors. Full-depth water ocean profiles could not be obtained for 8 weeks, between the March 14, 2020, and May 16, 2020, casts, due to the collapse of the PS hydrohole (Figure 7). As explained earlier, opening a new hole was not deemed feasible. Loss of this hydrohole had further impact on sampling not only of the deep but also of the upper and intermediate layers, due to limited sample volume of the OC-CTD. As the ice was already thin and melting when Leg 4 started in early June, Ocean City was not fully reestablished, so no OC-CTD sampling was carried out after about mid-May. This situation had the largest impact on the shallow measurements (e.g., nitrate and CDOM) and sampling, which could only be carried out within the limitations of the influence of the *Polarstern* hull on the upper water column. Undisturbed temperature and salinity data, and several bio-optical variables, could be measured during Legs 4 and 5 by the MSS, however. Finally, as the drift proceeded faster than expected, the camp had to be re-installed on a second ice floe during Leg 5. Much of the equipment was redeployed then (Figure 7), except for the turbulence cluster, the MR, the Aural and all equipment from the first ridge site. As in other parts of the Central Observatory, the first ridge site experienced severe deformation during Leg 3, which led to difficulties in accessing the site for data download, the eventual loss of several of the instruments, and thus data gaps in the “Fort Ridge” ADCP and CTD observations (Figure 7). Due to the

deformation across the Central Observatory, the AOFB/Pycnocline Spar obtained observations of vertical fluxes and horizontal velocity only until mid-March, with later operations again during Leg 5.

Despite these gaps, the observational data in Figure 7 highlight several concurrent measurements to study local and regional feedbacks within the coupled Arctic climate system, in particular:

- vertical energy budgets at the ice-ocean interface, the under-ice mixed layer and the upper halocline (heat and momentum; e.g., Shaw et al., 2009; Fer et al., 2017) during Legs 2–3, using the AOFB/Pycnocline Spar, turbulence cluster, MR, ADCP (various), and MSS;
- sub-mesoscale and mesoscale horizontal variability and internal waves (e.g., Manucharyan and Thompson, 2017) during Legs 1–4, using the turbulence cluster and MSS;
- ridge hydrodynamics (e.g., Skyllingstad et al., 2003) for several weeks during Leg 2, using the CTD RBR and ADCP Signature 1000, and during Leg 5 using the Nortek Vector and Nortek Aquadopp;
- vertical fluxes of different measured variables and sampled substances (e.g., Randelhoff et al., 2020) during Legs 1–3, using the MSS and OC-CTD, and during Legs 4–5, using the MSS and PS-CTD; and
- water masses throughout the water column; and related to large-scale advection and local modification by mixing, double-diffusion and entrainment.

In addition to regular observations there are several sets of intensified measurements during various events. One example is provided in Section 5, and further details will be available in the general MOSAiC overview (additional overview article expected in this special collection, led by M Rex).

5. Preliminary results

5.1. Hydrographic properties during the five legs

We present the CTD profiles down to 2000 m, with the data median-averaged in time for each leg (Figure 8; 1 dbar ~=1 m). Starting at the surface, all temperature profiles are similarly close to freezing in the top 40 m, except for Leg 5 (purple) which is above the freezing point of seawater, as expected for a summer profile. This is also the least saline at the surface, due to ice melt. The vertical differences in salinity are more pronounced than those in temperature and underline differences in the mixed layer from leg to leg: the mixed layer deepens from, on average, shallower than 40 m in Legs 1 (red) and 2 (yellow) to 60 m in Leg 3 (green). The top 100 m of Leg 4 (blue) differ from the other legs primarily because of regional, not seasonal, differences: Leg 4 was spent mostly over the Yermak Plateau and in Fram Strait.

Figure 8.

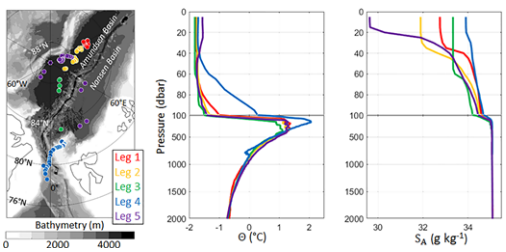

View large Download slide

Hydrographic properties during the five legs . Left: location of all of the full-depth casts with the Polarstern-hydrohole-CTD during the Multidisciplinary drifting Observatory for the Study of the Arctic Climate drift, color-coded per leg; bathymetry from GEBCO (Weatherall et al., 2020). Right: for each leg, corresponding CTD profiles of conservative temperature (Θ) and absolute salinity (S_A), median-averaged in time for each leg and vertically averaged into 5-dbar bins (1 dbar 1 m). CTD data are preliminary and available in Tippenhauer et al. (2021) . Number of casts, distance, and time period differ for each leg (see Figure 7). CTD = conductivity-temperature profiling through depth. DOI: https://doi.org/10.1525/elementa.2021.00062.f8

Deeper than 100 m, differences in all profiles are most likely reflective of the regionality in the Arctic. Between depths of 100 and 500 m, the Atlantic Water is warmest during Leg 4, i.e. near its inflow to the Arctic. As expected in the Amundsen Basin, as we sampled from east to west, the Atlantic Water temperature decreases from Leg 1 to 2, then 3 (see also T-S diagram in left panel, Figure 9). Leg 5 again sampled the region sampled by Leg 2, and consequently exhibits similar Atlantic Water temperatures.

Figure 9.

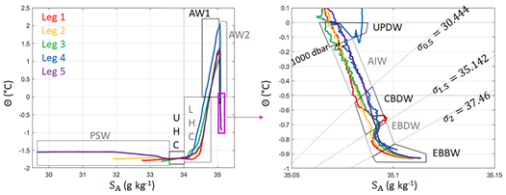

View large Download slide

Conservative temperature-absolute salinity diagram . Conservative temperature versus absolute salinity of the data shown in Figure 8, with the main water masses highlighted. Left panel, starting at the ocean surface: Polar Surface Water, Upper Halocline, Lower Halocline, Upper Atlantic Water, and Lower Atlantic Water (AW2). Deeper water masses in the magenta rectangle, zoomed in on the right panel, again starting at the shallowest just under AW2: Upper Polar Deep Water, Arctic Intermediate Water, Canada Basin Deep Water, Eurasian Basin Deep Water, and Eurasian Basin Bottom Water. See water mass definitions in Table S2. Number of casts, distance, and time period vary differ for each leg (see Figures 7 and 8). DOI: https://doi.org/10.1525/elementa.2021.00062.f9

Underneath the Atlantic Water layer, differences are most visible on a T-S diagram (right panel, Figure 9). The most interesting difference between the legs is the presence or absence of Canada Basin Deep Water intrusions, clearly visible as a local salinity maximum around 2000-m depth (see Leg 1 in red around –0.65°C on right panel, Figure 9). The distribution in properties of Eurasian Basin Deep Water and Eurasian Basin Bottom Water is somewhat surprising, with warmest and saltiest waters in Leg 4 as expected, but coldest and freshest in Leg 1, as if properties changed linearly from west to east in the Amundsen Basin, whereas we expected the opposite. More work investigating the properties of these water masses will appear in later publications, in particular comparing our MOSAiC measurements to the few existing historical casts and ongoing Synoptic Arctic Survey measurements.

5.2. Longer deployments: Upper ocean hydrography and currents

As detailed in section 3, hydrographic properties, in the upper ocean in particular, were measured by more sensors than the PS-CTD. Here we present data from an ITP that was located in the Distributed Network (Figure 10). Figure 10 shows the evolution of mixed-layer depth defined by a potential density difference of 0.05 kg m $^{-3}$ from the surface (e.g., Toole et al., 2010). The mixed layer became thicker during our drift from north of the

Laptev Sea toward the Yermak Plateau (January–April). This thickening was partly due to freezing and concurrent brine rejection, in turn leading to haline convection. There is a strong regional component as the ITP drifted into the region of the Fram Strait inflow of warm AW, where winter mixing reaches deeper than in the Eurasian central Arctic Ocean due to higher near-surface salinity and less stratification. The mixed-layer depth was much shallower than the upper bound of the warm AW, denoted by the 0°C isotherm, for much of the drift, except near the Fram Strait inflow (May onwards). The conditions near the Fram Strait inflow reflect the winter mixing in this region, where the lower halocline is formed. This lower halocline, denoted by the 34 g kg $^{-1}$ isohaline (Figure 10b), was within a few meters of the mixed layer near the beginning and the end of the section, but much shallower in the Eurasian central Arctic Ocean part of the Transpolar Drift. The halocline has been found to form not only close to the Fram Strait inflow north of Svalbard, but as far east as the Laptev Sea in recent years (Polyakov et al., 2017). We now appear to observe this signal further north in the basin, "downstream" of the boundary current at the continental slope of the Kara and Laptev seas.

Figure 10.

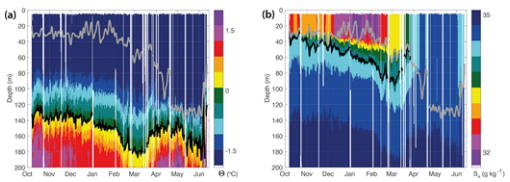

View large Download slide

Sections of hydrography along the drift track . Evolution of the (a) conservative temperature and (b) absolute salinity with depth (y-axis) and time along the Multidisciplinary drifting Observatory for the Study of the Arctic Climate drift track (x-axis) from twice-daily profiles by ITP #111 (Toole et al., 2016). The black line in (a) is the 0°C isotherm; in (b), the 34 g kg $^{-1}$ isohaline; see text for explanation. The gray line denotes the mixed-layer depth (see text) on both panels. Parts of the section without data are shown in white. The time series has been interpolated linearly to fill gaps in the top 20 m of the section and subsequently smoothed by a lowpass 5th-order Butterworth-Filter (cutoff period of 7 days; Butterworth, 1930), then again applying a mask to reflect measurement gaps (white areas in Figure 10). ITP #111 drifted with the Distributed Network around the Central Observatory; the system was recovered in July, but due to large data gaps, we only show the time series until June. DOI: https://doi.org/10.1525/elementa.2021.00062.f10

Here we present one example of a continuous time-series measurement at the Central Observatory: current velocities as measured by the 75 kHz ADCP. Current observations from Legs 1–3 support the well-known notion of a "quiescent" Arctic Ocean, with current speeds averaging 3.8 cm s $^{-1}$ and rarely exceeding 5 cm s $^{-1}$ (Figure 11). However, despite this overall sluggish nature, we observed several episodes with strongly increased upper-ocean velocities in early spring (March–April 2020), where current speeds exceeded 25 cm s $^{-1}$ in the upper 50 m. These events are presumably linked to strong atmospheric forcing; their interaction with ice mobility and mixing is yet to be analyzed. During June–July 2020 (Leg 4), over the Yermak Plateau and Fram Strait, currents averaged 12.4 cm s $^{-1}$. This region is a tidal hotspot with elliptic tidal currents (e.g., Padman et al., 1992). These are evident in our measurements that also show a strong and persistent southwestward flow. From August 2020 onward (Leg 5), in the Eurasian central Arctic Ocean, observed velocities were 5 cm s $^{-1}$, which is relatively larger than the average 3.8 cm s $^{-1}$ observed in the same region in winter (Legs 1–3). The bottom panel of Figure 11 shows that this increase is not confined to the upper ocean, but spreads throughout the observed water

column.

Figure 11.

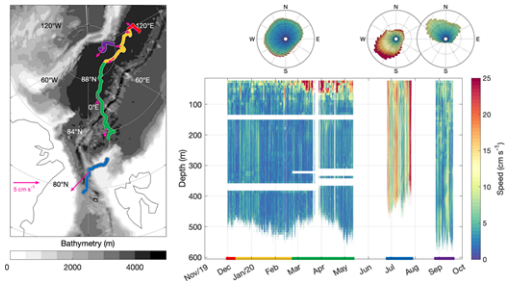

View large Download slide

Current velocity . Left panel, drift track (color-coded per leg, cf. bottom of right panel) with magenta arrows indicating vertically and monthly averaged velocity measured by the 75-kHz acoustic Doppler current profiler. Top right panel: current roses indicating prevalent directions (in 10° bins; greater distance from the center indicates greater occurrence) and speed (colors) for each of the three deployments. Bottom right panel: time-depth plot of current speed for each deployment. The data are available in Baumann et al. (2021) . DOI: https://doi.org/10.1525/elementa.2021.00062.f11

5.3. Event, targeted measurements: Meltwater layer in leads

Along with the routine measurements that produced the year-long time series shown above and detailed in Section 4, part of our profiling and sampling efforts were made in response to “events”, such as lead openings. During Legs 4 and 5, SST-CTD measurements in leads revealed the presence of a meltwater layer at the surface. This meltwater layer was also detected by other profiling instruments, not shown here as their calibration is ongoing. The presence of a meltwater layer at the surface during one such lead event on August 25, 2020, is clearly visible in Figure 12 . The temperature closely follows the salinity-dependent freezing point (panel a) and salinity is lower than 5 g kg $^{-1}$ at the very surface (panel b). Below the meltwater layer (panels c and d), the profile exhibits the typical temperature and salinity characteristics observed in the high Arctic, which are also described in Figure 9 : halocline close to freezing until approximately 100-m depth, with the comparatively warm Atlantic Water layer below. After the first large storm of Leg 5, on September 6, 2020, the meltwater layer was not observed in our measurements, implying a sensitivity to wind conditions. This storm was another “event” during which intense sampling was performed. In particular, the team collected microstructure profiles uninterrupted for a duration of 36 h.

Figure 12.

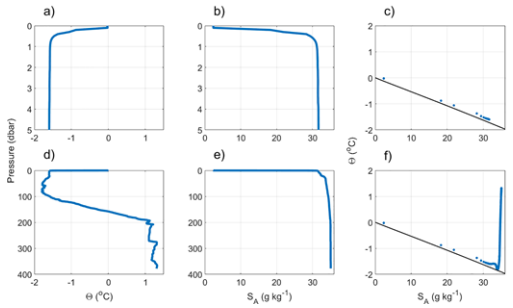

View large Download slide

Hydrography during melting. Vertical profiles of (a) conservative temperature (Θ) and (b) absolute salinity (S_A) for the top 5 dbar (ca 5 m) of the water column, (c)

combined as a Θ - S_A diagram along with freezing line (black), and (d) Θ and (e) S_A and (f) Θ - S_A diagram for the full profile, collected by the SST-CTD on August 25, 2020. The data are available in Tippenhauer et al. (2021). SST = Sea and Sun Technologies; CTD = conductivity-temperature profiling through depth. DOI: https://doi.org/10.1525/elementa.2021.00062.f12

6. Inside OCEAN and beyond: Linkages to modeling and observations by other teams

All MOSAiC teams have contributed to research on the wider climate system, in particular current climate change, either explicitly or via their relation to modeling. Many projects aim to investigate the response of the Arctic Ocean to the disappearance of perennial ice. Here we briefly relate the observations of Team OCEAN to those of other teams and to remote sensing and numerical modeling.

6.1. Relation to satellite retrieval

Team OCEAN observations can give added value to the analysis of various types of satellite observations, both by in-situ validation of satellite products and by analysis of combined datasets. Below we outline the relevant satellite missions and data products, and potential analyses.

Sea surface temperature (SST) in the Arctic has long been retrieved from infrared remote sensing (e.g., Key and Haefliger, 1992) at comparatively high spatial resolution (approximately 1 km) but only for cloud-free conditions, and in combination with microwave radiometers at lower resolution under all cloud conditions (e.g., Donlon et al., 2012). Usually, SST can only be retrieved in ice-free regions because separating SST from ice surface temperature for sea-ice leads narrower than the satellite footprint resolution is still a challenge (e.g., Fan et al., 2020). Our SST measurements throughout MOSAiC and, in particular, our measurements in leads (see Figure 12) can be used as validation data for satellite-based SST. Moreover, our SST measurements along with our microstructure measurements can improve the turbulent heat flux observed by these satellites (e.g., Qu et al., 2019). Our full-depth hydrography data can be used as validation for satellite gravimetry. Combined with satellite altimetry, improved gravimetry would reduce uncertainty in sea-level trends (e.g., Jeon et al., 2018) and allow us to monitor freshwater changes and geostrophic circulation in the Arctic with improved accuracy (e.g., Armitage et al., 2016, 2017; Doglioni et al., 2021).

Not only can our measurements be used as "ground truth", they also produce values or reveal physics that can be implemented in the satellite retrieval algorithms to improve the resulting products. For example, sea-ice thickness and sea-ice production retrievals assume that the ocean temperature is very close to freezing (e.g., Ricker et al., 2017), yet our measurements during Leg 4 showed instances where the ocean under the ice was significantly above freezing. The ocean temperature measurements can also be used in combination with satellite retrievals to partition the oceanic and atmospheric forcing to the sea-ice volume decline (Ricker et al., 2021). Satellite products of air-sea fluxes, notably of carbon, require information about upper ocean turbulence (e.g., Buchwitz et al., 2018), which is assumed to be low in the Arctic. Our extensive turbulence measurements during MOSAiC, and their preliminary results indicating that the Arctic is far from being as "quiet" as traditionally assumed (see Section 5), may force such products to change their parameterization. Our turbulence and under-ice current measurements can also be used to evaluate satellite sea-ice drag products (Heorton et al., 2019), and will be combined in future studies with ICESat-2 satellite laser altimeter data.

On the other hand, we expect satellite retrievals to be of great use to complement our ocean observations. Of most immediate relevance to the MOSAiC physical oceanographers will be the use of satellite sea-ice products in combination with observations from the Central Observatory and the Distributed Network to analyze the ocean's response to different ice conditions. Sea-ice drift and deformation products, in particular, from high resolution Synthetic Aperture Radar (SAR) sensors (Krumpen et al., 2021), can provide us with a detailed map of estimated under-ice currents over the entire Distributed Network and beyond, not just at the locations that we instrumented. Most of Team OCEAN measurements were taken under ice, but some were taken in leads as well as in the presence of open water areas in spring and summer. Satellite measurements can help to upscale these local observations to a regional scale. From spaceborne infrared (MODIS, AMSR) and SAR data, one can detect leads (e.g., Murashkin et al., 2018 ; Reiser et al., 2020), where new ice formation is highly relevant to changes in ocean mixed-layer properties; from SAR and/or altimetry, one can detect eddies (e.g., Kozlov et al., 2019 ; Bashmachnikov et al., 2020). SAR can also reveal the surface signature of internal waves (e.g., Thompson and Gasparovic, 1986). All of these applications would allow us to place our observations, in particular those across the Distributed Network, into a larger geographical context.

6.2. Relation to modeling

MOSAiC physical oceanography observations provide a basis for a step-change in understanding the Arctic dynamics and motivating further model improvements. The following aspects are of particular relevance to modelling:

– The observations cover the seasonal cycle across a large part of the Eurasian central Arctic Ocean, often at high temporal resolution for specific processes (e.g., 36-h uninterrupted MSS series), ranging from mixed layer variability to turbulent mixing, double diffusion, and internal waves;

– Several measurements encompass an entire basin full-depth, from the surface to the seafloor, and as such can be used to identify biases in a model's representation of the mixed layer depth, vertical stratification and water mass characteristics over the full annual cycle of atmospheric and sea-ice conditions;

– The observations are not only point measurements from *Polarstern* , but also from Ocean City and the Distributed Network, thus allowing a meaningful comparison to the model values representative of a grid cell;

– Measurements were taken in coordination with all of the other teams, allowing an interdisciplinary approach to study coupled processes and feedbacks of the ocean, ice and air, radiative/heat /freshwater budgets, turbulent fluxes, carbon cycle, nutrient transports, and trace gas pathways, among others; and

– The conditions during 2020 were unique, with an extremely rapid transpolar ice drift, lower sea-ice thicknesses with potential impacts on the transport of the ice-rafted material across the Arctic, stronger oceanic connectivity between the western Siberian shelves and the central Arctic Ocean and a record shift from an extremely low to an extremely high Arctic Oscillation in winter (Dethloff et al., 2021 ; Krumpen et al., 2021 ; Rinke et al., 2021 ; Wilson et al., 2021).

This set of year-long MOSAiC physical oceanography data is expected to advance understanding of physical processes in the ocean and their role in coupling with the sea ice and atmosphere. The leading goal is to provide more robust assessments of the current changes in all of the components of the Arctic system. The results can facilitate more reliable seasonal to decadal prediction and better projection of the future changes in the Arctic. Two ways to achieve this goal is by improving sub-grid-scale process representation and by accounting for the new key emerging processes not previously considered in the models. The MOSAiC observations are instrumental for these developments, and they are initially being used to evaluate and tune ocean and fully coupled climate models, with a focus on improving the representation of coupled processes. In particular, the under-ice ocean measurements obtained during winter and the transitional seasons constitute unique measurements for process-oriented model evaluation and calibration. These include observations of: air-ice-ocean radiative, turbulent and momentum fluxes; inertial oscillations; mixed layer dynamics; and turbulent mixing. They may lead to better parameterisations of the vertical fluxes of heat, mass and momentum and improved simulations of the upper ocean content of fresh water and heat (Solomon et al., 2021); double diffusion, which is one of the dominating processes in the water mass transformation in the present Arctic climate (Guthrie et al., 2017); mixing due to internal waves (e.g., Dosser et al., 2021); and barotropic and baroclinic currents, and eddies (Armitage et al., 2020 ; Timmermans and Marshall, 2020). Work that combines observational analysis and modeling is currently evaluating biases in an hierarchy of models, from regional high-resolution (sub-kilometer scale) ice-ocean and coupled models to global coupled models from the Climate Model Intercomparison Project phase 6 (CMIP6; Eyring et al., 2016). The MOSAiC data are to make a central contribution to this activity. Another example of the joint modeling and observational effort is to examine sub-mesoscale and mesoscale eddy statistics, and to improve their parameterization using data and high-resolution modeling (e.g., Danilov et al., 2017 ; Kubryakov et al., 2021). A further aspect is to explore large-scale dynamical structures in the surface ice and ocean flows (Wilson et al., 2021). On the interdisciplinary side, ongoing modeling of the pan-Arctic advection of heat, nutrients, and other biogeochemically relevant substances by sea ice and ocean gives crucial input to predict the near future of the Arctic in response to climate change (e.g., Ardyna and Arrigo, 2020 ; Krumpen et al., 2020 ; Belter et al., 2021). Ocean data assimilation and state estimation, in the form of hindcasts using adjoint methods or an ocean reanalysis, is another important focus of modeling research (e.g., Nguyen et al., 2021).

6.3. The coupled system: Relation to disciplinary in-situ observations

The MOSAiC expedition has been unique in the sense that all observations were planned with the aim of observing the fully coupled Arctic atmosphere-ice-ocean system (general MOSAiC overview, article expected in this special collection, led by M Rex). Consequently, the physical oceanography measurements strongly contribute to answering transdisciplinary research questions. We here give a few examples of ongoing studies (see also Table S1) and an outlook into the future.

The physical oceanography observations can be combined with those of snow, sea-ice, and atmospheric processes and properties to enable characterization of the complete heat, freshwater, and momentum budgets of the coupled ocean-ice-atmosphere physical system. The unique MOSAiC observational dataset will allow us to close these budgets for different

seasons and different ice conditions, in particular in the marginal ice zone and in the transitional seasons. We can observe, for example, the large heat loss from the ocean to the atmosphere in winter, both through leads and conduction through the sea ice (e.g., McPhee and Untersteiner, 1982); conversely, the solar heating in summer via open water and transmission through the sea ice. These heat fluxes influence the ocean mixed-layer temperature, the rate of winter ice growth and the amount of summer bottom melt. One result of winter cooling on the under-ice ocean mixed layer has already highlighted for the first time the formation of platelet ice in winter (Katlein et al., 2020). There is, further, an indication that the impact of upper ocean heat on reduced ice growth is currently increasing (Ricker et al., 2021). Such cross-cutting analyzes can also examine the momentum transfer during storms via atmosphere-ice-ocean interaction, and freshwater gain into the ocean as the ice melts in summer.

Another topic of importance for all MOSAiC teams is the exchange of climate-relevant gases. Measurements of CH_4, N_2O and dimethylsulfide in the winter mixed layer will shed light on the still unconsidered exchange of these dissolved gases at the ice-sea interface coupled to brine release during freezing and ice growth as alternative pathways to the ice-atmospheric gas fluxes during winter. Measurements from the OC-CTD will be augmented by those from the PS-CTD, from our installations on the ice, and from the Distributed Network, and will provide additional information about the ocean's capability to absorb these gases. Of particular importance are observations of temperature and vertical mixing. On the large scale, the deeper water column of the Arctic Ocean may be an important sink for methane, previously released from the Arctic seabed on the shelves (Shakhova et al., 2014) and transported within sea ice to the interior Arctic (Damm et al., 2018; Verdugo et al., 2021). Currently, there is a strong imbalance between bottom-up and top-down estimates of methane sources and sinks (AMAP, 2015). Although observations of methane flux to the atmosphere from leads in the ice-covered ocean have been reported (Kort et al., 2012; Berchet et al., 2016), Lower Halocline and Atlantic Water (Figure 9) may facilitate methane oxidation. The capacity of this sink depends heavily on the circulation time scale and production of cold waters through shelf-basin exchange, because microbial oxidation in the Arctic is slow (Damm et al., 2015; Uhlig and Loose, 2017). A suite of water mass tracers have also been sampled in collaboration by the OCEAN and BGC teams (see Section 3.b). The results will be used for common studies on, for example, riverine influence (Bauch et al., 2011; Laukert et al., 2017b, 2019; Paffrath et al., 2021) or water mass ventilation (Rhein et al., 2017). In general, estimates of upper-ocean processes —vertical turbulent kinetic energy, dissipation, ice-water current shear, convection from brine drainage and heat flux between the ocean and the atmosphere, are all important determinants of air-water and ice-water gas exchange. These estimates are limited primarily by turbulence on the water side of these interfaces (Lovely, 2014; Loose et al., 2016). The measurements of these physical processes throughout can help to connect the observations of gas flux to the physical drivers that produce them.

Physical processes also shape and influence Arctic ecosystem properties and processes. The range of impacts can span from fine-scale effects on under-ice organismal dispersal around ridged ice blocks to mesoscale processes that shape regional microbial community structure. Furthermore, water mass properties can inform observed patterns in ecosystem-wide distributions of species, from viruses to fish (Gradinger et al., 2010; Wassmann, 2015). Within MOSAiC, a broad suite of ecological properties and rates were measured coinciding with hydrographic

measurements to address gaps in our understanding of how organisms and their metabolisms respond to the seasonal and spatial changes in ocean dynamics. In part, the physical state of the ocean determines the distributions of essential nutrients and dissolved compounds, which are vital to supporting Arctic life, and partially structures interactions between organisms and their environment (Polyakov et al., 2013). Additionally, physical conditions can drive changes in organismal, population-wide, and community-level aspects of ecosystem processes and functions, thereby playing an important role in the interpretation of observed responses and/or shifts in the Arctic ecosystem (Slagstad et al., 2015). Resolving the especially tight coupling between upper ocean dynamics, sea ice, and biological activities is critical to addressing time- and space-sensitive responses of the Arctic ecosystem (Wassmann, 2015), and is one example of how ocean physics link ecosystem measurements to broader processes of the Arctic climate system.

7. Conclusions

We presented the scientific background, planning, and field setup of the physical oceanography work during the MOSAiC expedition. Our setup had to be modified due to environmental conditions, such as ice deformation, extremely cold temperature and seasonal melt. In addition, COVID-19 interrupted personnel rotation. Despite these odds, we managed to obtain a comprehensive year-round set of data observed in the ocean, some ranging from under the sea ice to the seafloor. Much of the instrumentation worked across the Eurasian Basin and throughout all seasons. The data obtained during the drift have been partly processed and analyzed after the expedition, already showing the added value of the numerous observations that were carried out regularly and in parallel, within our "Team OCEAN" and in collaboration with the other teams. All data will be publicly available by January 2023 at the latest.

The data presented in Section 5 highlight the large-scale nature of our observations as well as the resolution we were able to obtain, both in time and space, to study local processes in detail. Targeted observations allowed us to resolve specific event-driven phenomena that cannot easily be studied by traditional research icebreaker surveys, due to the associated spatial focus and limited ship time.

Many process studies facilitated by the observations will guide future satellite missions and lead to model improvements. This effort includes the development of ocean-related model parameterizations and ocean coupling with other climate system components. Further, our experience regarding the implementation of such ambitious and complex fieldwork, coordinated across many countries and teams both on- and off-shore, will be extremely useful to future Arctic Ocean fieldwork. Overall, the data collected by Team OCEAN will be the main legacy of the physical oceanography work within the MOSAiC expedition, which will enable many uniquely physical and interdisciplinary analyses over the coming years.

Data accessibility statement

All data are archived in the Multidisciplinary drifting Observatory for the Study of the Arctic Climate Central Storage (MCS) and will be available at the time of final publication in the data repositories PANGAEA and the Arctic Data Center. Additional references to data sets that are already publicly available are given in the text. All other data shown in this work will be published during the review process and will be available by the time of acceptance.

Supplemental files

The supplemental files for this article can be found as follows:

Text S1 . Details of instruments and methods.

Table S1 . Table of contributing projects.

Table S2 . Definition of water masses represented in Figure 9 .

Acknowledgments

This work was carried out and data used in this manuscript were produced as part of the international Multidisciplinary drifting Observatory for the Study of the Arctic Climate (MOSAiC) with the tag MOSAiC20192020 (AWI_PS122_00). We thank all those who contributed to MOSAiC and made this endeavor possible (Nixdorf et al., 2021). We thank the two anonymous reviewers for their useful comments that helped to improve this manuscript.

Funding

The following projects and funding agencies contributed to this work:

– Why is the deep Arctic Ocean Warming is funded by the Swedish Research Council, project number 2018-03859, and berth fees for this project were covered by the Swedish Polar Research Secretariat;

– The Changing Arctic Ocean (CAO) program, jointly funded by the United Kingdom Research and Innovation (UKRI) Natural Environment Research Council (NERC) and the Bundesministerium für Bildung und Forschung (BMBF), in particular, the CAO projects Advective Pathways of nutrients and key Ecological substances in the ARctic (APEAR) grants NE/R012865/1, NE/R012865/2, and #03V01461, and the project Primary productivity driven by Escalating Arctic NUTrient fluxeS grant #03F0804A;

– The Research Council of Norway (AROMA, grant no 294396; HAVOC, grant no 280292; and CAATEX, grant no 280531);

– Collaborative Research: Thermodynamics and Dynamic Drivers of the Arctic Sea Ice Mass Budget at Multidisciplinary drifting Observatory for the Study of the Arctic Climate; National Science Foundation (NSF) projects 1723400, Stanton; OPP-1724551, Shupe;

– The Helmholtz society strategic investment Frontiers in Arctic Marine monitoring (FRAM);

– Deutsche Forschungsgemeinschaft (German Research Foundation) through the Transregional Collaborative Research Centre TRR 172 “ArctiC Amplification: Climate Relevant Atmospheric and SurfaCe Processes, and Feedback Mechanisms (AC)3” (grant 268020496);

– The Japan Society for the Promotion of Science (grant numbers JP18H03745, JP18KK0292, and JP17KK0083) and the COLE grant of U. Tokyo;

– National Key Research and Development Plan Sub-Project of Ministry of Science and Technology of China (2016YFA0601804), “Simulation, Prediction and Regional Climate Response of Global Warming Hiatus”, 2016/07-2021/06;

– National Science Foundation grant number OPP-1756100 which

funded two of the Ice-Tethered Profilers and all the Ice-Tethered Profiler deployments;

– Chinese Polar Environmental Comprehensive Investigation and Assessment Programs, funded by the Chinese Arctic and Antarctic Administration; Marine Science and Technology Fund of Shandong Province for Qingdao National Laboratory for Marine Science and Technology (Grant: 2018SDKJ0104-1) and Chinese Natural Science Foundation (Grant: 41941012);

– UK NERC Long-term Science Multiple Centre National Capability Programme "North Atlantic Climate System Integrated Study (ACSIS)", grant NE/N018044/1;

– The London NERC Doctoral Training Partnership grant (NE/L002485/1) which funded RDCM;

– NSF grant number OPP-1753423, which funded the ^{7}Be tracer –measurements; and

– The Alfred-Wegener-Institut Helmholtz-Zentrum für Polar- und Meeresforschung (AWI) through its projects: AWI_OCEAN, AWI_ROV, AWI_ICE, AWI_SNOW, AWI_ECO, AWI_ATMO, and AWI_BGC.

Competing interests

All authors declare that they have no competing interests.

Author contributions

Contributed to conception and design: AAF, AR, AS, ArS, BK, BL, BR, CH, CM, ChH, DB, DC, DK, DP, DVD, ED, GL, GS, HH, HL, HW, IF, IK, JKO, JMT, JR, JZ, JiR, JiS, JiZ, KD, KS, LL, LW, LiL, MAG, MH, MJ, ML, MN, MR, MDS, MV, MW, MZ, MaW, MoM, NL, RAK, RG, RL, ST, STC, TK, ThK, TL, TS, VM, VS, WM, WS, XM, YA, YF, YH, YK, YW, ZK.

Contributed to acquisition of data: AAF, AD, AR, AS, BK, BR, CB, ChH, DB, DK, DVD, ED, FD, FE, GS, HH, HL, HW, IK, IS, JA, JR, JS, JiR, JiZ, KS, LC, LL, LW, MA, MH, ML, MM, MN, MR, MDS, MaW, MoM, NR, NS, RDCM, RL, RM, SK, KT, ST, TK, ThK, TL, TS, VM, VS, WS, XM, YB, YF, ZK.

Contributed to analysis and interpretation of data: AAF, AR, BL, BR, CH, ChH, DB, DK, DP, ED, GS, HL, IF, IK, JR, JS, KD, KS, LiL, MAG, MH, MJ, MN, MR, MDS, MV, MW, MaW, NR, RG, SK, ST, TK, TL, TMB, TS, WM, YA, YF, YK, ZK.

Drafted and/or revised this article: All authors.

Approved the submitted version for publication: All authors.

References

Aagaard, K, Johnson, JM. 2011. The North Pole environmental observatory mooring. *Oceanography* 24(3): 100–101. DOI: http://dx.doi.org/10.5670/oceanog.2011.60. Google Scholar

Alford, MH, MacKinnon, JA, Simmons, HL, Nash, JD. 2016. Near-inertial internal gravity waves in the ocean. *Annual Review of Marine Science* 8(1): 95–123. DOI: http://dx.doi.org/10.1146/annurev-marine-010814-015746. Google Scholar

Alfred-Wegener-Institut Helmholtz-Zentrum für Polar- und Meeresforschung. 2017. Polar research and supply vessel POLARSTERN operated by the Alfred-Wegener-Institute. *Journal of Large-Scale Research Facilities* 3: A119. DOI: http://dx.doi.org/10.17815/jlsrf-3-163.

AMAP Assessment. 2015. *Methane as an Arctic climate forcer*. Oslo, Norway: Arctic

Monitoring and Assessment Programme (AMAP): vii + 139.

Ardyna, M, Arrigo, KR. 2020. Phytoplankton dynamics in a changing Arctic Ocean. *Nature Climate Change* 10: 892–903. DOI: http://dx.doi.org/10.1038/s41558-020-0905-y.
Google Scholar

Armitage, TWK, Bacon, S, Ridout, AL, Petty, AA, Wolbach, S, Tsamados, M. 2017. Arctic Ocean surface geostrophic circulation 2003–2014. *The Cryosphere* 11(4): 1767–1780. DOI: http://dx.doi.org/10.5194/tc-11-1767-2017.
Google Scholar

Armitage, TWK, Bacon, S, Ridout, AL, Thomas, SF, Aksenov, Y, Wingham, DJ. 2016. Arctic sea surface height variability and change from satellite radar altimetry and GRACE, 2003–2014. *Journal of Geophysical Research: Oceans* 121(6): 4303–4322. DOI: http://dx.doi.org/10.1002/2015JC011579.
Google Scholar

Armitage, TWK, Manucharyan, GE, Petty, AA, Kwok, R, Thompson, AF. 2020. Enhanced eddy activity in the Beaufort Gyre in response to sea ice loss. *Nature Communications* 11(1): 761. DOI: http://dx.doi.org/10.1038/s41467-020-14449-z.
Google Scholar

Arrigo, KR, van Dijken, GL. 2011. Secular trends in Arctic Ocean net primary production. *Journal of Geophysical Research: Oceans* 116(C9). DOI: http://dx.doi.org/10.1029/2011JC007151.
Google Scholar

Athanase, M, Sennéchael, N, Garric, G, Koenig, Z, Boles, E, Provost, C. 2019. New hydrographic measurements of the upper Arctic western Eurasian Basin in 2017 reveal fresher mixed layer and shallower warm layer than 2005–2012 climatology. *Journal of Geophysical Research: Oceans* 124(2): 1091–1114. DOI: http://dx.doi.org/10.1029/2018JC014701.
Google Scholar

Ballinger, TJ, Overland, JE, Wang, M, Bhatt, US, Hanna, E, Hanssen-Bauer, I, Kim, SJ, Thoman, RL, Walsh, JE. 2020. Arctic Report Card 2020: Surface air temperature. DOI: http://dx.doi.org/10.25923/gcw8-2z06.
Google Scholar

Bashmachnikov, IL, Kozlov, IE, Petrenko, LA, Glok, NI, Wekerle, C. 2020. Eddies in the North Greenland Sea and Fram Strait from satellite altimetry, SAR and high-resolution model data. *Journal of Geophysical Research: Oceans* 125(7). DOI: http://dx.doi.org/10.1029/2019JC015832.
Google Scholar

Bauch, D, van der Loeff, MR, Andersen, N, Torres-Valdes, S, Bakker, K, Abrahamsen, EP. 2011. Origin of freshwater and polynya water in the Arctic Ocean halocline in summer 2007. *Progress in Oceanography* 91(4): 482–495. DOI: http://dx.doi.org/10.1016/j.pocean.2011.07.017.
Google Scholar

Baumann, T, Fer, I, Bryhni, H, Peterson, AK, Allerholt, J, Fang, Y-C, Hoppmann, M, Karam, S, Koenig, Z, Kong, B, Mohrholz, V, Muilwijk, M, Schaffer, J, Schulz, K, Sukhikh, N, Tippenhauer, S. 2021. Under-ice current measurements during MOSAiC from a 75 kHz acoustic Doppler profiler [dataset]. Available at http://doi.org/10.1594/PANGAEA.934792.
Google Scholar

Behrendt, A, Sumata, H, Rabe, B, Schauer, U. 2018. UDASH—Unified database for Arctic and subarctic hydrography. *Earth System Science Data* 10(2): 1119–1138. DOI: http://dx.doi.org/10.5194/essd-10-1119-2018.
Google Scholar

Belter, HJ, Krumpen, T, von Albedyll, L, Alekseeva, TA, Birnbaum, G, Frolov, SV, Hendricks, S, Herber, A, Polyakov, I, Raphael, I, Ricker, R, Serovetnikov, SS, Webster, M, Haas, C. 2021. Interannual variability in Transpolar Drift summer sea ice thickness and potential impact of Atlantification. *The Cryosphere* 15(6): 2575–2591. DOI: http://dx.doi.org/10.5194/tc-15-2575-2021.
Google Scholar

Berchet, A, Bousquet, P, Pison, I, Locatelli, R, Chevallier, F, Paris, JD,

Dlugokencky, EJ, Laurila, T, Hatakka, J, Viisanen, Y, Worthy, DEJ, Nisbet, E, Fisher, R, France, J, Lowry, D, Ivakhov, V, Hermansen, O. 2016. Atmospheric constraints on the methane emissions from the East Siberian Shelf. *Atmospheric Chemistry and Physics* 16(6): 4147–4157. DOI: http://dx.doi.org/10.5194/acp-16-4147-2016.
Google Scholar

Biddle, LC, Swart, S. 2020. The observed seasonal cycle of submesoscale processes in the Antarctic marginal ice zone. *Journal of Geophysical Research: Oceans* 125(6): e2019JC015587. DOI: http://dx.doi.org/10.1029/2019JC015587.
Google Scholar

Boyer, TP, Baranova, OK, Coleman, C, Garcia, HE, Grodsky, A, Locarnini, RA, Mishonov, AV, Paver, CR, Reagan, JR, Seidov, D, Smolyar, IV, Weathers, KW, Zweng, MM. 2018. World Ocean Database 2018, in Mishonov, AV, Technical Editor. NOAA Atlas NESDIS 87.
Google Scholar

Buchwitz, M, Reuter, M, Schneising, O, Noël, S, Gier, B, Bovensmann, H, Burrows, JP, Boesch, H, Anand, J, Parker, RJ, Somkuti, P, Detmers, RG, Hasekamp, OP, Aben, I, Butz, A, Kuze, A, Suto, H, Yoshida, Y, Crisp, D, O'Dell, C. 2018. Computation and analysis of atmospheric carbon dioxide annual mean growth rates from satellite observations during 2003–2016. *Atmospheric Chemistry and Physics* 18(23): 17355–17370. DOI: http://dx.doi.org/10.5194/acp-18-17355-2018.
Google Scholar

Bulsiewicz, K, Rose, H, Klatt, O, Putzka, A, Roether, W. 1998. A capillary-column chromatographic system for efficient chlorofluorocarbon measurement in ocean waters. *Journal of Geophysical Research: Oceans* 103(C8): 15959–15970. DOI: http://dx.doi.org/10.1029/98JC00140.
Google Scholar

Butterworth, S. 1930. On the theory of filter amplifiers. *Wireless Engineer / Experimental* 7: 536–541.
Google Scholar

Cohen, J, Zhang, X, Francis, J, Jung, T, Kwok, R, Overland, J, Ballinger, TJ, Bhatt, US, Chen, HW, Coumou, D, Feldstein, S, Gu, H, Handorf, D, Henderson, G, Ionita, M, Kretschmer, M, Laliberte, F, Lee, S, Linderholm, HW, Maslowski, W, Peings, Y, Pfeiffer, K, Rigor, I, Semmler, T, Stroeve, J, Taylor, PC, Vavrus, S, Vihma, T, Wang, S, Wendisch, M, Wu, Y, Yoon, J. 2020. Divergent consensuses on Arctic amplification influence on midlatitude severe winter weather. *Nature Climate Change* 10(1): 20–29. DOI: http://dx.doi.org/10.1038/s41558-019-0662-y.
Google Scholar

Damm, E, Bauch, D, Krumpen, T, Rabe, B, Korhonen, M, Vinogradova, E, Uhlig, C. 2018. The Transpolar Drift conveys methane from the Siberian Shelf to the central Arctic Ocean. *Scientific Reports* 8: 4515. DOI: http://dx.doi.org/10.1038/s41598-018-22801-z.
Google Scholar

Damm, E, Rudels, B, Schauer, U, Mau, S, Dieckmann, G. 2015. Methane excess in Arctic surface water-triggered by sea ice formation and melting. *Scientific Reports* 5: 16179. DOI: http://dx.doi.org/10.1038/srep16179.
Google Scholar

Danilov, S, Sidorenko, D, Wang, Q, Jung, T. 2017. The Finite-volumE Sea ice–Ocean Model (FESOM2). *Geoscientific Model Development* 10(2): 765–789. DOI: http://dx.doi.org/10.5194/gmd-10-765-2017.
Google Scholar

Dethloff, K, Maslowski, W, Hendricks, S, Lee, Y, Goessling, HF, Krumpen, T, Haas, C, Handorf, D, Ricker, R, Bessonov, V, Cassano, JJ, Kinney, JC, Osinski, R, Rex, M, Rinke, A, Sokolova, J, Sommerfeld, A. 2021. Arctic sea ice anomalies during the MOSAiC winter 2019/20. *The Cryosphere Discussion* 2021: 1–33. DOI: http://dx.doi.org/10.5194/tc-2020-375.
Google Scholar

Doglioni, F, Ricker, R, Rabe, B, Kanzow, T. 2021. Sea surface height anomaly and geostrophic velocity from altimetry measurements over the Arctic Ocean (2011–2018). *Earth System Science Data Discussion* 2021: 1–46. DOI: http://dx.doi.org

/10.5194/essd-2021-170.
Google Scholar

Donlon, CJ, Martin, M, Stark, J, Roberts-Jones, J, Fiedler, E, Wimmer, W. 2012. The operational sea surface temperature and sea ice analysis (OSTIA) system. *Remote Sensing of Environment* 116: 140–158. DOI: http://dx.doi.org/10.1016/j.rse.2010.10.017.
Google Scholar

Dosser, HV, Chanona, M, Waterman, S, Shibley, NC, Timmermans, M-L. 2021. Changes in internal wave-driven mixing across the Arctic Ocean: Finescale estimates from an 18-year Pan-Arctic record. *Geophysical Research Letters* 48(8): e2020GL091747. DOI: http://dx.doi.org/10.1029/2020GL091747.
Google Scholar

Eyring, V, Bony, S, Meehl, GA, Senior, CA, Stevens, B, Stouffer, RJ, Taylor, KE. 2016. Overview of the Coupled Model Intercomparison Project phase 6 (CMIP6) experimental design and organization. *Geoscientific Model Development* 9(5): 1937–1958. DOI: http://dx.doi.org/10.5194/gmd-9-1937-2016.
Google Scholar

Fan, P, Pang, X, Zhao, X, Shokr, M, Lei, R, Qu, M, Ji, Q, Ding, M. 2020. Sea ice surface temperature retrieval from Landsat 8/TIRS: Evaluation of five methods against in situ temperature records and MODIS IST in Arctic region. *Remote Sensing of Environment* 248: 111975. DOI: http://dx.doi.org/10.1016/j.rse.2020.111975.
Google Scholar

Fer, I. 2009. Weak vertical diffusion allows maintenance of cold halocline in the Central Arctic. *Atmospheric and Oceanic Science Letters* 2(3): 148–152. DOI: http://dx.doi.org/10.1080/16742834.2009.11446789.
Google Scholar

Fer, I. 2014. Near-inertial mixing in the Central Arctic Ocean. *Journal of Physical Oceanography* 44(8): 2031–2049. DOI: http://dx.doi.org/10.1175/jpo-d-13-0133.1.
Google Scholar

Fer, I, Peterson, AK, Randelhoff, A, Meyer, A. 2017. One-dimensional evolution of the upper water column in the Atlantic sector of the Arctic Ocean in winter. *Journal of Geophysical Research: Oceans* 122(3): 1665–1682. DOI: http://dx.doi.org/10.1002/2016JC012431.
Google Scholar

Florindo-López, C, Bacon, S, Aksenov, Y, Chafik, L, Colbourne, E, Holliday, NP. 2020. Arctic Ocean and Hudson Bay freshwater exports: New estimates from seven decades of hydrographic surveys on the Labrador Shelf. *Journal of Climate* 33(20): 8849–8868. DOI: http://dx.doi.org/10.1175/jcli-d-19-0083.1.
Google Scholar

Frolov, IE, Gudkovich, ZM, Radionov, VF, Shirochkov, AV, Timokhov, LA. 2005. *The Arctic Basin—Results from the Russian Drifting Stations*. Berlin, Germany: Springer.
Google Scholar

Gommenginger, C, Chapron, B, Hogg, A, Buckingham, C, Fox-Kemper, B, Eriksson, L, Soulat, F, Ubelmann, C, Ocampo-Torres, F, Nardelli, BB, Griffin, D, Lopez-Dekker, P, Knudsen, P, Andersen, O, Stenseng, L, Stapleton, N, Perrie, W, Violante-Carvalho, N, Schulz-Stellenfleth, J, Woolf, D, Isern-Fontanet, J, Ardhuin, F, Klein, P, Mouche, A, Pascual, A, Capet, X, Hauser, D, Stoffelen, A, Morrow, R, Aouf, L, Breivik, Ø, Fu, L-L, Johannessen, JA, Aksenov, Y, Bricheno, L, Hirschi, J, Martin, ACH, Martin, AP, Nurser, G, Polton, J, Wolf, J, Johnsen, H, Soloviev, A, Jacobs, GA, Collard, F, Groom, S, Kudryavtsev, V, Wilkin, J, Navarro, V, Babanin, A, Martin, M, Siddorn, J, Saulter, A, Rippeth, T, Emery, B, Maximenko, N, Romeiser, R, Graber, H, Azcarate, AA, Hughes, CW, Vandemark, D, Silva, Jd, Leeuwen, PJV, Naveira-Garabato, A, Gemmrich, J, Mahadevan, A, Marquez, J, Munro, Y, Doody, S, Burbidge, G. 2019. SEASTAR: A mission to study ocean submesoscale dynamics and small-scale atmosphere-ocean processes in coastal, shelf and polar seas. *Frontiers in Marine Science* 6(457). DOI: http://dx.doi.org/10.3389/fmars.2019.00457.
Google Scholar

Gradinger, R, Bluhm, B, Iken, K. 2010. Arctic sea-ice ridges—Safe heavens for sea-

ice fauna during periods of extreme ice melt? *Deep Sea Research Part II: Topical Studies in Oceanography* 57(1-2): 86–95. DOI: http://dx.doi.org/10.1016/j.dsr2.2009.08.008.
Google Scholar

Graham, RM, Itkin, P, Meyer, A, Sundfjord, A, Spreen, G, Smedsrud, LH, Liston, GE, Cheng, B, Cohen, L, Divine, D, Fer, I, Fransson, A, Gerland, S, Haapala, J, Hudson, SR, Johansson, AM, King, J, Merkouriadi, I, Peterson, AK, Provost, C, Randelhoff, A, Rinke, A, Rösel, A, Sennéchael, N, Walden, VP, Duarte, P, Assmy, P, Steen, H, Granskog, MA. 2019. Winter storms accelerate the demise of sea ice in the Atlantic sector of the Arctic Ocean. *Scientific Reports* 9(1): 9222. DOI: http://dx.doi.org/10.1038/s41598-019-45574-5.
Google Scholar

Granskog, MA, Fer, I, Rinke, A, Steen, H. 2018. Atmosphere-ice-ocean-ecosystem processes in a thinner Arctic sea ice regime: The Norwegian young sea ICE (N-ICE2015) expedition. *Journal of Geophysical Research: Oceans* 123(3): 1586–1594. DOI: http://dx.doi.org/10.1002/2017JC013328.
Google Scholar

Guthrie, JD, Fer, I, Morison, JH. 2017. Thermohaline staircases in the Amundsen Basin: Possible disruption by shear and mixing. *Journal of Geophysical Research: Oceans* 122(10): 7767–7782. DOI: http://dx.doi.org/10.1002/2017JC012993.
Google Scholar

Guthrie, JD, Morison, JH. 2021. Not just sea ice: Other factors important to near-inertial wave generation in the Arctic Ocean. *Geophysical Research Letters* 48(3): e2020GL090508. DOI: http://dx.doi.org/10.1029/2020GL090508.
Google Scholar

Haas, C, Hoppmann, M, Tippenhauer, S, Rohardt, G. 2021. Continuous thermosalinograph oceanography along RV POLARSTERN cruise track PS122/2 [dataset]. Available at http://doi.org/10.1594/PANGAEA.930024.
Google Scholar

Haine, TWN, Curry, B, Gerdes, R, Hansen, E, Karcher, M, Lee, C, Rudels, B, Spreen, G, de Steur, L, Stewart, KD, Woodgate, R. 2015. Arctic freshwater export: Status, mechanisms, and prospects. *Global and Planetary Change* 125: 13–35. DOI: http://dx.doi.org/10.1016/j.gloplacha.2014.11.013.
Google Scholar

Haine, TWN, Martin, T. 2017. The Arctic-subarctic sea ice system is entering a seasonal regime: Implications for future Arctic amplification. *Scientific Reports* 7(1): 4618. DOI: http://dx.doi.org/10.1038/s41598-017-04573-0.
Google Scholar

Hatakeyama, K, Hosono, M, Shimada, K, Kikuchi, T, Nishino, S. 2001. JAMSTEC Compact Arctic Drifter (J-CAD): A new generation drifting buoy to observe the Arctic Ocean. *Journal of the Japan Society for Marine Surveys and Technology* 13(1): 1_55–1_68. DOI: http://dx.doi.org/10.11306/jsmst.13.1_55.
Google Scholar

Heorton, HDBS, Tsamados, M, Cole, ST, Ferreira, AMG, Berbellini, A, Fox, M, Armitage, TWK. 2019. Retrieving sea ice drag coefficients and turning angles from in situ and satellite observations using an inverse modeling framework. *Journal of Geophysical Research: Oceans* 124(8): 6388–6413. DOI: http://dx.doi.org/10.1029/2018JC014881.
Google Scholar

Ilıcak, M, Drange, H, Wang, Q, Gerdes, R, Aksenov, Y, Bailey, D, Bentsen, M, Biastoch, A, Bozec, A, Böning, C, Cassou, C, Chassignet, E, Coward, AC, Curry, B, Danabasoglu, G, Danilov, S, Fernandez, E, Fogli, PG, Fujii, Y, Griffies, SM, Iovino, D, Jahn, A, Jung, T, Large, WG, Lee, C, Lique, C, Lu, J, Masina, S, George Nurser, AJ, Roth, C, Salas y Mélia, D, Samuels, BL, Spence, P, Tsujino, H, Valcke, S, Voldoire, A, Wang, X, Yeager, SG. 2016. An assessment of the Arctic Ocean in a suite of interannual CORE-II simulations. Part III: Hydrography and fluxes. *Ocean Modelling* 100: 141–161. DOI: http://dx.doi.org/10.1016/j.ocemod.2016.02.004.
Google Scholar

Intergovernmental Panel on Climate Change. 2013. *Climate change 2013: The physical science basis*. Contribution of Working Group I to the Fifth Assessment

Report of the Intergovernmental Panel on Climate Change. Cambridge, UK: Cambridge University Press.

Itoh, M, Shimada, K. 2003. *XCTD salinity calibration in the Arctic Ocean*. Yokosuka, Japan: JAMSTEC.

Ivanov, V, Varentsov, M, Matveeva, T, Repina, I, Artamonov, A, Khavina, E. 2019. Arctic sea ice decline in the 2010s: The increasing role of the ocean–air heat exchange in the late summer. *Atmosphere* 10(4): 184. DOI: http://dx.doi.org/10.3390/atmos10040184.
Google Scholar

Jeon, T, Seo, K-W, Youm, K, Chen, J, Wilson, CR. 2018. Global sea level change signatures observed by GRACE satellite gravimetry. *Scientific Reports* 8(1): 13519. DOI: http://dx.doi.org/10.1038/s41598-018-31972-8.
Google Scholar

Kadko, D, Galfond, B, Landing, WM, Shelley, RU. 2016. Determining the pathways, fate, and flux of atmospherically derived trace elements in the Arctic ocean/ice system. *Marine Chemistry* 182: 38–50. DOI: http://dx.doi.org/10.1016/j.marchem.2016.04.006.
Google Scholar

Kanzow, T, Hoppmann, M, Tippenhauer, S, Rohardt, G. 2021. Continuous thermosalinograph oceanography along RV POLARSTERN cruise track PS122/3 [dataset]. Available at http://dx.doi.org/10.1594/PANGAEA.930026.
Google Scholar

Katlein, C, Mohrholz, V, Sheikin, I, Itkin, P, Divine, DV, Stroeve, J, Jutila, A, Krampe, D, Shimanchuk, E, Raphael, I, Rabe, B, Kuznetsov, I, Mallet, M, Liu, H, Hoppmann, M, Fang, Y-C, Dumitrascu, A, Arndt, S, Anhaus, P, Nicolaus, M, Matero, I, Oggier, M, Eicken, H, Haas, C. 2020. Platelet ice under Arctic pack ice in winter. *Geophysical Research Letters* 47(16): e2020GL088898. DOI: http://dx.doi.org/10.1029/2020GL088898.
Google Scholar

Kawaguchi, Y, Nishino, S, Inoue, J. 2015. Fixed-point observation of mixed layer evolution in the seasonally ice-free Chukchi Sea: Turbulent mixing due to gale winds and internal gravity waves. *Journal of Physical Oceanography* 45(3): 836–853. DOI: http://dx.doi.org/10.1175/JPO-D-14-0149.1.
Google Scholar

Key, J, Haefliger, M. 1992. Arctic ice surface temperature retrieval from AVHRR thermal channels. *Journal of Geophysical Research: Atmospheres* 97(D5): 5885–5893. DOI: http://dx.doi.org/10.1029/92JD00348.
Google Scholar

Kikuchi, T, Inoue, J, Langevin, D. 2007. Argo-type profiling float observations under the Arctic multiyear ice. *Deep Sea Research Part I: Oceanographic Research Papers* 54(9): 1675–1686. DOI: http://dx.doi.org/10.1016/j.dsr.2007.05.011.
Google Scholar

Kilic, L, Prigent, C, Aires, F, Boutin, J, Heygster, G, Tonboe, RT, Roquet, H, Jimenez, C, Donlon, C. 2018. Expected performances of the Copernicus Imaging Microwave Radiometer (CIMR) for an all-weather and high spatial resolution estimation of ocean and sea ice parameters. *Journal of Geophysical Research: Oceans* 123(10): 7564–7580. DOI: http://dx.doi.org/10.1029/2018JC014408.
Google Scholar

Koenig, Z, Provost, C, Villacieros-Robineau, N, Sennéchael, N, Meyer, A. 2016. Winter ocean-ice interactions under thin sea ice observed by IAOOS platforms during N-ICE2015: Salty surface mixed layer and active basal melt. *Journal of Geophysical Research: Oceans* 121(10): 7898–7916. DOI: http://dx.doi.org/10.1002/2016JC012195.
Google Scholar

Korhonen, M, Rudels, B, Marnela, M, Wisotzki, A, Zhao, J. 2013. Time and space variability of freshwater content, heat content and seasonal ice melt in the Arctic Ocean from 1991 to 2011. *Ocean Science* 9(6): 1015–1055. DOI: http://dx.doi.org/10.5194/os-9-1015-2013.
Google Scholar

Kort, EA, Wofsy, SC, Daube, BC, Diao, M, Elkins, JW, Gao, RS, Hintsa, EJ, Hurst, DF, Jimenez, R, Moore, FL, Spackman, JR, Zondlo, MA. 2012. Atmospheric observations of Arctic Ocean methane emissions up to 82° north. *Nature Geoscience* 5(5): 318–321. DOI: http://dx.doi.org/10.1038/ngeo1452.
Google Scholar

Kozlov, IE, Artamonova, AV, Manucharyan, GE, Kubryakov, AA. 2019. Eddies in the western Arctic Ocean from spaceborne SAR observations over open ocean and marginal ice zones. *Journal of Geophysical Research: Oceans* 124(9): 6601–6616. DOI: http://dx.doi.org/10.1029/2019JC015113.
Google Scholar

Krishfield, RA, Perovich, DK. 2005. Spatial and temporal variability of oceanic heat flux to the Arctic ice pack. *Journal of Geophysical Research: Oceans* 110(C7). DOI: http://dx.doi.org/10.1029/2004JC002293.
Google Scholar

Krumpen, T, Belter, HJ, Boetius, A, Damm, E, Haas, C, Hendricks, S, Nicolaus, M, Noethig, E-M, Paul, S, Peeken, I, Ricker, R, Stein, R. 2019. Arctic warming interrupts the Transpolar Drift and affects long-range transport of sea ice and ice-rafted matter. *Scientific Reports* 9(1): 5459. DOI: http://dx.doi.org/10.1038/s41598-019-41456-y.
Google Scholar

Krumpen, T, Birrien, F, Kauker, F, Rackow, T, von Albedyll, L, Angelopoulos, M, Belter, HJ, Bessonov, V, Damm, E, Dethloff, K, Haapala, J, Haas, C, Harris, C, Hendricks, S, Hoelemann, J, Hoppmann, M, Kaleschke, L, Karcher, M, Kolabutin, N, Lei, R, Lenz, J, Morgenstern, A, Nicolaus, M, Nixdorf, U, Petrovsky, T, Rabe, B, Rabenstein, L, Rex, M, Ricker, R, Rohde, J, Shimanchuk, E, Singha, S, Smolyanitsky, V, Sokolov, V, Stanton, T, Timofeeva, A, Tsamados, M, Watkins, D. 2020. The MOSAiC ice floe: Sediment-laden survivor from the Siberian shelf. *The Cryosphere* 14(7): 2173–2187. DOI: http://dx.doi.org/10.5194/tc-14-2173-2020.
Google Scholar

Krumpen, T, von Albedyll, L, Goessling, HF, Hendricks, S, Juhls, B, Spreen, G, Willmes, S, Belter, HJ, Dethloff, K, Haas, C, Kaleschke, L, Katlein, C, Tian-Kunze, X, Ricker, R, Rostosky, P, Rückert, J, Singha, S, Sokolova, J. 2021. MOSAiC drift expedition from October 2019 to July 2020: Sea ice conditions from space and comparison with previous years. *The Cryosphere* 15(8): 3897–3920. DOI: http://dx.doi.org/10.5194/tc-15-3897-2021.
Google Scholar

Kubryakov, AA, Kozlov, IE, Manucharyan, GE. 2021. Large mesoscale eddies in the western Arctic Ocean from satellite altimetry measurements. *Journal of Geophysical Research: Oceans* 126(5): e2020JC016670. DOI: http://dx.doi.org/10.1029/2020JC016670.
Google Scholar

Laukert, G, Frank, M, Bauch, D, Hathorne, EC, Rabe, B, von Appen, W-J, Wegner, C, Zieringer, M, Kassens, H. 2017a. Ocean circulation and freshwater pathways in the Arctic Mediterranean based on a combined Nd isotope, REE and oxygen isotope section across Fram Strait. *Geochimica et Cosmochimica Acta* 202: 285–309. DOI: http://dx.doi.org/10.1016/j.gca.2016.12.028.
Google Scholar

Laukert, G, Frank, M, Bauch, D, Hathorne, EC, Gutjahr, M, Janout, M, Hölemann, J. 2017b. Transport and transformation of riverine Neodymium isotope and rare earth element signatures in high latitude estuaries: A case study from the Laptev Sea. *Earth and Planetary Science Letters* 477: 205–217 DOI: http://dx.doi.org/10.1016/j.epsl.2017.08.010.
Google Scholar

Laukert, G, Frank, M, Hathorne, EC, Krumpen, T, Rabe, B, Bauch, D, Werner, K, Peeken, I, Kassens, H. 2017c. Pathways of Siberian freshwater and sea ice in the Arctic Ocean traced with radiogenic Neodymium isotopes and rare earth elements. *Polarforschung* 87(1): 3–13. DOI: http://dx.doi.org/ 10.2312/polarforschung.87.1.3.
Google Scholar

Laukert, G, Makhotin, M, Petrova, MV, Frank, M, Hathorne, EC, Bauch, D, Böning, P, Kassens, H. 2019. Water mass transformation in the Barents Sea inferred from radiogenic neodymium isotopes, rare earth elements and stable oxygen

isotopes. *Chemical Geology* 511: 416–430. DOI: http://dx.doi.org/10.1016/j.chemgeo.2018.10.002.
Google Scholar

Lee, CM, Thomson, J, The Marginal Ice Zone Team, The Arctic Sea State Team. 2017. An autonomous approach to observing the seasonal ice zone in the western Arctic. *Oceanography* 30(2): 56–68.
Google Scholar Crossref

Lehner, F, Raible, CC, Hofer, D, Stocker, TF. 2012. The freshwater balance of polar regions in transient simulations from 1500 to 2100 AD using a comprehensive coupled climate model. *Climate Dynamics* 39(1): 347–363. DOI: http://dx.doi.org/10.1007/s00382-011-1199-6.
Google Scholar

Levine, MD. 1990. Internal waves under the Arctic pack ice during the Arctic Internal Wave Experiment: The coherence structure. *Journal of Geophysical Research: Oceans* 95(C5): 7347–7357. DOI: http://dx.doi.org/10.1029/JC095iC05p07347.
Google Scholar

Levine, MD, Paulson, CA, Morison, JH. 1985. Internal waves in the Arctic Ocean: Comparison with lower-latitude observations. *Journal of Physical Oceanography* 15: 800–809. DOI: http://dx.doi.org/10.1175/1520-0485(1985)015<0800:IWITAO>2.0.CO;2.
Google Scholar

Lévy, M, Franks, PJS, Smith, KS. 2018. The role of submesoscale currents in structuring marine ecosystems. *Nature Communications* 9(1): 4758. DOI: http://dx.doi.org/10.1038/s41467-018-07059-3.
Google Scholar

Lévy, M, Iovino, D, Resplandy, L, Klein, P, Madec, G, Tréguier, AM, Masson, S, Takahashi, K. 2012. Large-scale impacts of submesoscale dynamics on phytoplankton: Local and remote effects. *Ocean Modelling* 43–44: 77–93 DOI: http://dx.doi.org/10.1016/j.ocemod.2011.12.003.
Google Scholar

Li, G, Cheng, L, Zhu, J, Trenberth, KE, Mann, ME, Abraham, JP. 2020. Increasing ocean stratification over the past half-century. *Nature Climate Change* 10(12): 1116–1123. DOI: http://dx.doi.org/10.1038/s41558-020-00918-2.
Google Scholar

Loose, B, Lovely, A, Schlosser, P, Zappa, C, McGillis, W, Perovich, D. 2016. Currents and convection cause enhanced gas exchange in the ice–water boundary layer. *Tellus B: Chemical and Physical Meteorology* 68(1): 32803. DOI: http://dx.doi.org/10.3402/tellusb.v68.32803.
Google Scholar

López-Dekker, P, Rott, H, Prats-Iraola, P, Chapron, B, Scipal, K, Witte, ED. 2019. Harmony: An earth explorer 10 mission candidate to observe land, ice, and ocean surface dynamics. *IGARSS 2019–2019 IEEE International Geoscience and Remote Sensing Symposium* 2019: 8381–8384. DOI: http://dx.doi.org/ 10.1109/IGARSS.2019.8897983.
Google Scholar

Lovely, A. 2014. The effects of sea ice on gas transfer velocities and gas partitioning between water and sea ice [Open Access master's theses]. Paper 354. DOI: https://doi.org/10.23860/thesis-lovely-ann-2014.
Google Scholar

Lowry, KE, Pickart, RS, Selz, V, Mills, MM, Pacini, A, Lewis, KM, Joy-Warren, HL, Nobre, C, van Dijken, GL, Grondin, P-L, Ferland, J, Arrigo, KR. 2018. Under-ice phytoplankton blooms inhibited by spring convective mixing in refreezing leads. *Journal of Geophysical Research: Oceans* 123(1): 90–109. DOI: http://dx.doi.org/10.1002/2016JC012575.
Google Scholar

Luneva, MV, Ivanov, VV, Tuzov, F, Aksenov, Y, Harle, JD, Kelly, S, Holt, JT. 2020. Hotspots of dense water cascading in the Arctic Ocean: Implications for the Pacific water pathways. *Journal of Geophysical Research: Oceans* 125(10): e2020JC016044. DOI: http://dx.doi.org/10.1029/2020JC016044.

Google Scholar

Manucharyan, GE, Thompson, AF. 2017. Submesoscale sea ice-ocean interactions in marginal ice zones. *Journal of Geophysical Research: Oceans* 122(12): 9455–9475. DOI: http://dx.doi.org/10.1002/2017JC012895.
Google Scholar

Martin, T, Tsamados, M, Schroeder, D, Feltham, DL. 2016. The impact of variable sea ice roughness on changes in Arctic Ocean surface stress: A model study. *Journal of Geophysical Research: Oceans* 121(3): 1931–1952. DOI: http://dx.doi.org/10.1002/2015JC011186.
Google Scholar

McDougall, TJ, Barker, PM. 2011. *Getting started with TEOS-10 and the Gibbs Seawater (GSW) Oceanographic Toolbox*. SCOR/IAPSO WG127.
Google Scholar

McDougall, TJ, Feistel, R, Millero, F, Jackett, DR, Wright, D, King, B, Marion, G, Chen, C-TA, Spitzer, P. 2010. *The international thermodynamic equation of seawater 2010 (teos-10): Calculation and use of thermodynamic properties* Manuals and Guides 56 Intergovernmental Oceanographic Commission IOC of Unesco
Google Scholar

McPhee, MG, Kwok, R, Robins, R, Coon, M. 2005. Upwelling of Arctic pycnocline associated with shear motion of sea ice. *Geophysical Research Letters* 32(10). DOI: http://dx.doi.org/10.1029/2004GL021819.
Google Scholar

McPhee, MG, Untersteiner, N. 1982. Using sea ice to measure vertical heat flux in the ocean. *Journal of Geophysical Research: Oceans* 87(C3): 2071–2074. DOI: http://dx.doi.org/10.1029/JC087iC03p02071.
Google Scholar

Meredith, M, Sommerkorn, M, Cassotta, S, Derksen, C, Ekaykin, A, Hollowed, A, Kofinas, G, Mackintosh, A, Melbourne-Thomas, J, Muelbert, MMC, Ottersen, G, Pritchard, H, Schuur, EAG. 2019. Polar regions, in Pörtner, H-O, Roberts, DC, Masson-Delmotte, V, Zhai, P, Tignor, M, Poloczanska, E, Mintenbeck, K, Alegría, A, Nicolai, M, Okem, A, Petzold, J, Rama, B, Weyer, NM eds., *IPCC special report on the ocean and cryosphere in a changing climate*, in press. Available at https://www.ipcc.ch/srocc/chapter/chapter-3-2/.

Meyer, A, Fer, I, Sundfjord, A, Peterson, AK. 2017. Mixing rates and vertical heat fluxes north of Svalbard from Arctic winter to spring. *Journal of Geophysical Research: Oceans* 122(6): 4569–4586. DOI: http://dx.doi.org/10.1002/2016JC012441.
Google Scholar

Meyer, H, Schönicke, L, Wand, U, Hubberten, HW, Friedrichsen, H. 2000. Isotope studies of hydrogen and oxygen in ground ice—Experiences with the equilibration technique. *Isotopes in Environmental and Health Studies* 36(2): 133–149. DOI: http://dx.doi.org/10.1080/10256010008032939.
Google Scholar

Morison, J, Aagaard, K, Falkner, KK, Hatakeyama, K, Moritz, R, Overland, JE, Perovich, D, Shimada, K, Steele, M, Takizawa, T, Woodgate, R. 2002. North Pole Environmental Observatory delivers early results. *Eos, Transactions American Geophysical Union* 83(33): 357–361. DOI: http://dx.doi.org/10.1029/2002EO000259.
Google Scholar

Murashkin, D, Spreen, G, Huntemann, M, Dierking, W. 2018. Method for detection of leads from Sentinel-1 SAR images. *Annals of Glaciology* 59(76pt2): 124–136. DOI: http://dx.doi.org/10.1017/aog.2018.6.
Google Scholar

Nansen, F. 1902. *The oceanography of the North Polar Basin*. Christiania, Norway: Dybwad.
Google Scholar

Nguyen, AT, Pillar, H, Ocaña, V, Bigdeli, A, Smith, TA, Heimbach, P. 2021. The Arctic Subpolar Gyre sTate estimate: Description and assessment of a data-constrained, dynamically consistent ocean-sea ice estimate for 2002–2017. *Journal of Advances in Modeling Earth Systems* 13(5): e2020MS002398. DOI: http://dx.doi.org/10.1029/2020MS002398.

Google Scholar

Nicolaus, M, Perovich, DK, Spreen, G, Granskog, MA, Albedyll, Lv, Angelopoulos, M, Anhaus, P, Arndt, S, Belter, HJ, Bessonov, V, Birnbaum, G, Brauchle, J, Calmer, R, Cardellach, E, Cheng, B, Clemens-Sewall, D, Dadic, R, Damm, E, Boer, Gd, Demir, O, Dethloff, K, Divine, DV, Fong, AA, Fons, S, Frey, M, Fuchs, N, Gabarró, C, Gerland, S, Goessling, HF, Gradinger, R, Haapala, J, Haas, C, Hamilton, J, Hannula, H-R, Hendricks, S, Herber, A, Heuzé, C, Hoppmann, M, Høyland, KV, Huntemann, M, Hutchings, JK, Hwang, B, Itkin, P, Jacobi, H-W, Jaggi, M, Jutila, A, Kaleschke, L, Katlein, C, Kolabutin, N, Krampe, D, Kristensen, SS, Krumpen, T, Kurtz, N, Lampert, A, Lange, BA, Lei, R, Light, B, Linhardt, F, Liston, GE, Loose, B, Macfarlane, AR, Mahmud, M, Matero, IO, Maus, S, Morgenstern, A, Naderpour, R, Nandan, V, Niubom, A, Oggier, M, Oppelt, N, Pätzold, F, Perron, C, Petrovsky, T, Pirazzini, R, Polashenski, C, Rabe, B, Raphael, IA, Regnery, J, Rex, M, Ricker, R, Riemann-Campe, K, Rinke, A, Rohde, J, Salganik, E, Scharien, RK, Schiller, M, Schneebeli, M, Semmling, M, Shimanchuk, E, Shupe, MD, Smith, MM, Smolyanitsky, V, Sokolov, V, Stanton, T, Stroeve, J, Thielke, L, Timofeeva, A, Tonboe, RT, Tavri, A, Tsamados, M, Wagner, DN, Watkins, D, Webster, M, Wendisch, M. 2022. Overview of the MOSAiC expedition: Snow and sea ice. *Elementa: Science of the Anthropocene* 10(1). DOI: https://doi.org/10.1525/elementa.2021.000046.
Google Scholar

Nishino, S, Kikuchi, T, Yamamoto-Kawai, M, Kawaguchi, Y, Hirawake, T, Itoh, M. 2011. Enhancement/reduction of biological pump depends on ocean circulation in the sea-ice reduction regions of the Arctic Ocean. *Journal of Oceanography* 67(3): 305–314. DOI: http://dx.doi.org/10.1007/s10872-011-0030-7.
Google Scholar

Nixdorf, U, Dethloff, K, Rex, M, Shupe, M, Sommerfeld, A, Perovich, D, Nicolaus, M, Heuzé, C, Rabe, B, Loose, B, Damm, E, Gradinger, R, Fong, A, Maslowski, W, Rinke, A, Kwok, R, Spreen, G, Wendisch, M, Herber, A, Hirsekorn, M, Mohaupt, V, Frickenhaus, S, Immerz, A, Weiss-Tuider, K, König, B, Mengedoht, D, Regnery, J, Gerchow, P, Ransby, D, Krumpen, T, Morgenstern, A, Haas, C, Kanzow, T, Rack, FR, Saitzev, V, Sokolov, V, Makarov, A, Schwarze, S, Wunderlich, T, Wurr, K, Boetius, A. 2021. MOSAiC extended acknowledgement. Zenodo. DOI: http://dx.doi.org/10.5281/zenodo.5179738.
Google Scholar

Nurser, AJG, Bacon, S. 2014. The Rossby radius in the Arctic Ocean. *Ocean Science* 10(6): 967–975. DOI: http://dx.doi.org/10.5194/os-10-967-2014.
Google Scholar

Padman, L, Plueddemann, AJ, Muench, RD, Pinkel, R. 1992. Diurnal tides near the Yermak Plateau. *Journal of Geophysical Research: Oceans* 97(C8): 12639–12652. DOI: http://dx.doi.org/10.1029/92JC01097.
Google Scholar

Paffrath, R, Laukert, G, Bauch, D, van der Loeff, MR, Pahnke, K. 2021. Separating individual contributions of major Siberian rivers in the Transpolar Drift of the Arctic Ocean. *Scientific Reports* 11(1): 8216. DOI: http://dx.doi.org/10.1038/s41598-021-86948-y.
Google Scholar

Perovich, D, Meier, W, Tschudi, M, Hendricks, S, Petty, AA, Divine, D, Farrell, S, Gerland, S, Haas, C, Kaleschke, L, Pavlova, O, Ricker, R, Tian-Kunze, X, Webster, M, Wood, K. 2020. Arctic Report Card 2020: Sea Ice. DOI: http://dx.doi.org/10.25923/n170-9h57.
Google Scholar

Perovich, DK, Andreas, WL, Curry, JA, Eicken, H, Fairall, CW, Grenfell, TC, Guest, PS, Intrieri, J, Kadko, D, Lindsay, RW, McPhee, MG, Morison, J, Moritz, RE, Paulson, CA, Pegau, WS, Persson, POG, Pinkel, R, Richter-Menge, J, Stanton, T, Stern, H, Sturm, M, TuckerIII, WB, Uttal, T. 1999. Year on ice gives climate insights. *Eos Transactions* 80(41): 485–486.
Google Scholar Crossref

Perovich, DK, Moritz, RE. 2002. Preface. *Journal of Geophysical Research: Oceans* 107(C10): SHE 1-1–SHE 1-2. DOI: http://dx.doi.org/10.1029/2002JC001314.
Google Scholar

Pesant, S, Not, F, Picheral, M, Kandels-Lewis, S, Le Bescot, N, Gorsky, G, Iudicone, D, Karsenti, E, Speich, S, Troublé, R, Dimier, C, Searson, S, Acinas, SG, Bork, P, Boss, E, Bowler, C, De Vargas, C, Follows, M, Gorsky, G, Grimsley, N, Hingamp, P, Iudicone, D, Jaillon, O, Kandels-Lewis, S, Karp-Boss, L, Karsenti, E, Krzic, U, Not, F, Ogata, H, Pesant, S, Raes, J, Reynaud, EG, Sardet, C, Sieracki, M, Speich, S, Stemmann, L, Sullivan, MB, Sunagawa, S, Velayoudon, D, Weissenbach, J, Wincker, P, Tara Oceans Consortium Coordinators. 2015. Open science resources for the discovery and analysis of Tara Oceans data. *Scientific Data* 2(1): 150023. DOI: http://dx.doi.org/10.1038/sdata.2015.23.
Google Scholar

Polyakov, IV, Alexeev, VA, Ashik, IM, Bacon, S, Beszczynska-Möller, A, Carmack, EC, Dmitrenko, IA, Fortier, L, Gascard, J-C, Hansen, E, Hölemann, J, Ivanov, VV, Kikuchi, T, Kirillov, S, Lenn, Y-D, McLaughlin, FA, Piechura, J, Repina, I, Timokhov, LA, Walczowski, W, Woodgate, R. 2011. Fate of early 2000s Arctic warm water pulse. *Bulletin of the American Meteorological Society* 92(5): 561–566. DOI: http://dx.doi.org/10.1175/2010bams2921.1.
Google Scholar

Polyakov, IV, Alkire, MB, Bluhm, BA, Brown, KA, Carmack, EC, Chierici, M, Danielson, SL, Ellingsen, I, Ershova, EA, Gårdfeldt, K, Ingvaldsen, RB, Pnyushkov, AV, Slagstad, D, Wassmann, P. 2020. Borealization of the Arctic Ocean in response to anomalous advection from Sub-Arctic seas. *Frontiers in Marine Science* 7(491). DOI: http://dx.doi.org/10.3389/fmars.2020.00491.
Google Scholar

Polyakov, IV, Bhatt, US, Walsh, JE, Abrahamsen, EP, Pnyushkov, AV, Wassmann, PF. 2013. Recent oceanic changes in the Arctic in the context of long-term observations. *Ecological Applications* 23(8): 1745–1764. DOI: http://dx.doi.org/10.1890/11-0902.1.
Google Scholar

Polyakov, IV, Pnyushkov, AV, Alkire, MB, Ashik, IM, Baumann, TM, Carmack, EC, Goszczko, I, Guthrie, J, Ivanov, VV, Kanzow, T, Krishfield, R, Kwok, R, Sundfjord, A, Morison, J, Rember, R, Yulin, A. 2017. Greater role for Atlantic inflows on sea-ice loss in the Eurasian Basin of the Arctic Ocean. *Science* 356(6335): 285. DOI: http://dx.doi.org/10.1126/science.aai8204.
Google Scholar

Polyakov, IV, Pnyushkov, AV, Rember, R, Ivanov, VV, Lenn, Y-D, Padman, L, Carmack, EC. 2012. Mooring-based observations of double-diffusive staircases over the Laptev Sea slope. *Journal of Physical Oceanography* 42(1): 95–109. DOI: http://dx.doi.org/10.1175/2011jpo4606.1.
Google Scholar

Proshutinsky, A, Krishfield, R, Toole, JM, Timmermans, M-L, Williams, W, Zimmermann, S, Yamamoto-Kawai, M, Armitage, TWK, Dukhovskoy, D, Golubeva, E, Manucharyan, GE, Platov, G, Watanabe, E, Kikuchi, T, Nishino, S, Itoh, M, Kang, S-H, Cho, K-H, Tateyama, K, Zhao, J. 2019. Analysis of the Beaufort Gyre freshwater content in 2003–2018. *Journal of Geophysical Research: Oceans* 124(12): 9658–9689. DOI: http://dx.doi.org/10.1029/2019JC015281.
Google Scholar

Qu, M, Pang, X, Zhao, X, Zhang, J, Ji, Q, Fan, P. 2019. Estimation of turbulent heat flux over leads using satellite thermal images. *The Cryosphere* 13(6): 1565–1582. DOI: http://dx.doi.org/10.5194/tc-13-1565-2019.
Google Scholar

Rabe, B, Karcher, M, Kauker, F, Schauer, U, Toole, JM, Krishfield, RA, Pisarev, S, Kikuchi, T, Su, J. 2014. Arctic Ocean basin liquid freshwater storage trend 1992–2012. *Geophysical Research Letters* 41(3): 961–968. DOI: http://dx.doi.org/10.1002/2013GL058121.
Google Scholar

Rabe, B, Karcher, M, Schauer, U, Toole, JM, Krishfield, RA, Pisarev, S, Kauker, F, Gerdes, R, Kikuchi, T. 2011. An assessment of Arctic Ocean freshwater content changes from the 1990s to the 2006–2008 period. *Deep Sea Research Part I: Oceanographic Research Papers* 58(2): 173–185. DOI: http://dx.doi.org/10.1016/j.dsr.2010.12.002.
Google Scholar

Randelhoff, A, Holding, J, Janout, M, Sejr, MK, Babin, M, Tremblay, J-É, Alkire, MB. 2020. Pan-Arctic Ocean primary production constrained by turbulent nitrate fluxes. *Frontiers in Marine Science* 7(150). DOI: http://dx.doi.org/10.3389/fmars.2020.00150.
Google Scholar

Reiser, F, Willmes, S, Heinemann, G. 2020. A new algorithm for daily sea ice lead identification in the Arctic and Antarctic winter from thermal-infrared satellite imagery. *Remote Sensing* 12(12): 1957. DOI: http://dx.doi.org/10.3390/rs12121957.
Google Scholar

Rex, M, Hoppmann, M, Tippenhauer, S, Rohardt, G. 2021a. Continuous thermosalinograph oceanography along RV POLARSTERN cruise track PS122/1 [dataset]. Available at http://doi.org/10.1594/PANGAEA.930023.
Google Scholar

Rex, M, Hoppmann, M, Tippenhauer, S, Rohardt, G. 2021b. Continuous thermosalinograph oceanography along RV POLARSTERN cruise track PS122/4 [dataset]. Available at http://doi.org/10.1594/PANGAEA.930027.
Google Scholar

Rex, M, Hoppmann, M, Tippenhauer, S, Rohardt, G. 2021c. Continuous thermosalinograph oceanography along RV POLARSTERN cruise track PS122/5 [dataset]. Available at http://doi.org/10.1594/PANGAEA.930028.
Google Scholar

Rhein, M, Steinfeldt, R, Kieke, D, Stendardo, I, Yashayaev, I. 2017. Ventilation variability of Labrador Sea water and its impact on oxygen and anthropogenic carbon: A review. *Philosophical Transactions of the Royal Society A: Mathematical, Physical and Engineering Sciences* 375(2102): 20160321. DOI: http://dx.doi.org/10.1098/rsta.2016.0321.
Google Scholar

Ricker, R, Hendricks, S, Girard-Ardhuin, F, Kaleschke, L, Lique, C, Tian-Kunze, X, Nicolaus, M, Krumpen, T. 2017. Satellite-observed drop of Arctic sea ice growth in winter 2015–2016. *Geophysical Research Letters* 44(7): 3236–3245. DOI: http://dx.doi.org/10.1002/2016gl072244.
Google Scholar

Ricker, R, Kauker, F, Schweiger, A, Hendricks, S, Zhang, J, Paul, S. 2021. Evidence for an increasing role of ocean heat in Arctic winter sea ice growth. *Journal of Climate* 34(13): 5215–5227. DOI: http://dx.doi.org/10.1175/jcli-d-20-0848.1.
Google Scholar

Rinke, A, Cassano, JJ, Cassano, EN, Jaiser, R, Handorf, D. 2021. Meteorological conditions during the MOSAiC expedition: Normal or anomalous? *Elementa: Science of the Anthropocene* 9(1). DOI: http://dx.doi.org/10.1525/elementa.2021.00023.
Google Scholar

Rudels, B. 2009. Arctic Ocean circulation, in Steele, J, Thorpe, S, Turekian, K eds., *Encyclopedia of ocean sciences*. 2nd ed. Oxford, UK: Academic Press: 211–225.
Google Scholar

Rudels, B, Korhonen, M, Schauer, U, Pisarev, S, Rabe, B, Wisotzki, A. 2015. Circulation and transformation of Atlantic water in the Eurasian Basin and the contribution of the Fram Strait inflow branch to the Arctic Ocean heat budget. *Progress in Oceanography* 132: 128–152. DOI: http://dx.doi.org/10.1016/j.pocean.2014.04.003.
Google Scholar

Rudels, B, Schauer, U, Björk, G, Korhonen, M, Pisarev, S, Rabe, B, Wisotzki, A. 2013. Observations of water masses and circulation with focus on the Eurasian Basin of the Arctic Ocean from the 1990s to the late 2000s. *Ocean Science* 9(1): 147–169. DOI: http://dx.doi.org/10.5194/os-9-147-2013.
Google Scholar

Schlitzer, R. 2015. Data analysis and visualization with Ocean Data View. *CMOS Bulletin SCMO* 43(1): 9–13.
Google Scholar

Shakhova, N, Semiletov, I, Leifer, I, Sergienko, V, Salyuk, A, Kosmach, D,

Chernykh, D, Stubbs, C, Nicolsky, D, Tumskoy, V, Gustafsson, Ö. 2014. Ebullition and storm-induced methane release from the East Siberian Arctic shelf. *Nature Geoscience* 7(1): 64–70. DOI: http://dx.doi.org/10.1038/ngeo2007.
Google Scholar

Shaw, WJ, Stanton, TP, McPhee, MG, Morison, JH, Martinson, DG. 2009. Role of the upper ocean in the energy budget of Arctic sea ice during SHEBA. *Journal of Geophysical Research: Oceans* 114(C6). DOI: http://dx.doi.org/10.1029/2008JC004991.
Google Scholar

Shirshov, P, Fedorov, E. 1938. Scientific work of the Drifting North Polar Station*. *Nature* 141(3571): 629–632. DOI: http://dx.doi.org/10.1038/141629a0.
Google Scholar

Shupe, MD, Rex, M, Blomquist, B, Persson, POG, Schmale, J, Uttal, T, Althausen, D, Angot, H, Archer, S, Bariteau, L, Beck, I, Bilberry, J, Bucci, S, Buck, C, Boyer, M, Brasseur, Z, Brooks, IM, Calmer, R, Cassano, J, Castro, V, Chu, D, Costa, D, Cox, CJ, Creamean, J, Crewell, S, Dahlke, S, Damm, E, de Boer, G, Deckelmann, H, Dethloff, K, Dütsch, M, Ebell, K, Ehrlich, A, Ellis, J, Engelmann, R, Fong, AA, Frey, MM, Gallagher, MR, Ganzeveld, L, Gradinger, R, Graeser, J, Greenamyer, V, Griesche, H, Griffiths, S, Hamilton, J, Heinemann, G, Helmig, D, Herber, A, Heuzé, C, Hofer, J, Houchens, T, Howard, D, Inoue, J, Jacobi, H-W, Jaiser, R, Jokinen, T, Jourdan, O, Jozef, G, King, W, Kirchgaessner, A, Klingebiel, M, Krassovski, M, Krumpen, T, Lampert, A, Landing, W, Laurila, T, Lawrence, D, Lonardi, M, Loose, B, Lüpkes, C, Maahn, M, Macke, A, Maslowski, W, Marsay, C, Maturilli, M, Mech, M, Morris, S, Moser, M, Nicolaus, M, Ortega, P, Osborn, J, Pätzold, F, Perovich, DK, Petäjä, T, Pilz, C, Pirazzini, R, Posman, K, Powers, H, Pratt, KA, Preußer, A, Quéléver, L, Radenz, M, Rabe, B, Rinke, A, Sachs, T, Schulz, A, Siebert, H, Silva, T, Solomon, A, Sommerfeld, A, Spreen, G, Stephens, M, Stohl, A, Svensson, G, Uin, J, Viegas, J, Voigt, C, von der Gathen, P, Wehner, B, Welker, JM, Wendisch, M, Werner, M, Xie, ZQ, Yue, F. 2022. Overview of the MOSAiC expedition: Atmosphere. *Elementa: Science of the Anthropocene* 10(1). DOI: https://doi.org/10.1525/elementa.2021.00060.
Google Scholar

Shupe, MD, Rex, M, Dethloff, K, Damm, E, Fong, AA, Gradinger, R, Heuzé, C, Loose, B, Makarov, A, Maslowski, W, Nicolaus, M, Perovich, D, Rabe, B, Rinke, A, Sokolov, V, Sommerfeld, A. 2020. Arctic Report Card 2020: The MOSAiC expedition: A year drifting with the Arctic sea ice. DOI: http://dx.doi.org/10.25923/9g3v-xh92.
Google Scholar

Skyllingstad, ED, Paulson, CA, Pegau, WS, McPhee, MG, Stanton, T. 2003. Effects of keels on ice bottom turbulence exchange. *Journal of Geophysical Research: Oceans* 108(C12). DOI: http://dx.doi.org/10.1029/2002JC001488.
Google Scholar

Slagstad, D, Wassmann, PFJ, Ellingsen, I. 2015. Physical constrains and productivity in the future Arctic Ocean. *Frontiers in Marine Science* 2(85). DOI: http://dx.doi.org/10.3389/fmars.2015.00085.
Google Scholar

Sloyan, BM, Wanninkhof, R, Kramp, M, Johnson, GC, Talley, LD, Tanhua, T, McDonagh, E, Cusack, C, O'Rourke, E, McGovern, E, Katsumata, K, Diggs, S, Hummon, J, Ishii, M, Azetsu-Scott, K, Boss, E, Ansorge, I, Perez, FF, Mercier, H, Williams, MJM, Anderson, L, Lee, JH, Murata, A, Kouketsu, S, Jeansson, E, Hoppema, M, Campos, E. 2019. The Global Ocean Ship-based Hydrographic Investigations Program (GO-SHIP): A platform for integrated multidisciplinary ocean science. *Frontiers in Marine Science* 6(445). DOI: http://dx.doi.org/10.3389/fmars.2019.00445.
Google Scholar

Smethie, WM, Chipman, DW, Swift, JH, Koltermann, KP. 1988. Chlorofluoromethanes in the Arctic Mediterranean seas: Evidence for formation of bottom water in the Eurasian Basin and deep-water exchange through Fram Strait. *Deep Sea Research Part A Oceanographic Research Papers* 35(3): 347–369. DOI: http://dx.doi.org/10.1016/0198-0149(88)90015-5.
Google Scholar

Solomon, A, Heuzé, C, Rabe, B, Bacon, S, Bertino, L, Heimbach, P, Inoue, J, Iovino, D, Mottram, R, Zhang, X, Aksenov, Y, McAdam, R, Nguyen, A, Raj, RP, Tang, H. 2021. Freshwater in the Arctic Ocean 2010–2019. *Ocean Science* 17(4): 1081–1102. DOI: http://dx.doi.org/10.5194/os-17-1081-2021.
Google Scholar

Somavilla, R, Schauer, U, Budéus, G. 2013. Increasing amount of Arctic Ocean deep waters in the Greenland Sea. *Geophysical Research Letters* 40(16): 4361–4366. DOI: http://dx.doi.org/10.1002/grl.50775.
Google Scholar

Stanton, TP, Shaw, WJ, Hutchings, JK. 2012. Observational study of relationships between incoming radiation, open water fraction, and ocean-to-ice heat flux in the Transpolar Drift: 2002–2010. *Journal of Geophysical Research: Oceans* 117(C7). DOI: http://dx.doi.org/10.1029/2011JC007871.
Google Scholar

Steele, M, Dickinson, S. 2016. The phenology of Arctic Ocean surface warming. *Journal of Geophysical Research: Oceans* 121(9): 6847–6861. DOI: http://dx.doi.org/10.1002/2016JC012089.
Google Scholar

Stopa, JE, Ardhuin, F, Girard-Ardhuin, F. 2016. Wave climate in the Arctic 1992–2014: Seasonality and trends. *The Cryosphere* 10(4): 1605–1629. DOI: http://dx.doi.org/10.5194/tc-10-1605-2016.
Google Scholar

Sültenfuß, J, Roether, W, Rhein, M. 2009. The Bremen mass spectrometric facility for the measurement of helium isotopes, neon, and tritium in water. *Isotopes in Environmental and Health Studies* 45(2): 83–95. DOI: http://dx.doi.org/10.1080/10256010902871929.
Google Scholar

Sumata, H, Kauker, F, Karcher, M, Rabe, B, Timmermans, ML, Behrendt, A, Gerdes, R, Schauer, U, Shimada, K, Cho, KH, Kikuchi, T. 2018. Decorrelation scales for Arctic Ocean hydrography—Part I: Amerasian Basin. *Ocean Science* 14(1): 161–185. DOI: http://dx.doi.org/10.5194/os-14-161-2018.
Google Scholar

Thoman, RL, Richter-Menge, J, Druckenmiller, ML. 2020. NOAA Arctic Report Card 2020 executive summary DOI: http://dx.doi.org/10.25923/mn5p-t549
Google Scholar

Thompson, DR, Gasparovic, RF. 1986. Intensity modulation in SAR images of internal waves. *Nature* 320(6060): 345–348.
Google Scholar Crossref

Timmermans, M-L, Cole, S, Toole, J. 2012. Horizontal density structure and restratification of the Arctic Ocean surface layer. *Journal of Physical Oceanography* 42(4): 659–668. DOI: http://dx.doi.org/10.1175/jpo-d-11-0125.1.
Google Scholar

Timmermans, M-L, Jayne, SR. 2016. The Arctic Ocean spices up. *Journal of Physical Oceanography* 46(4): 1277–1284. DOI: http://dx.doi.org/10.1175/jpo-d-16-0027.1.
Google Scholar

Timmermans, M-L, Marshall, J. 2020. Understanding Arctic Ocean circulation: A review of ocean dynamics in a changing climate. *Journal of Geophysical Research: Oceans* 125(4): e2018JC014378. DOI: http://dx.doi.org/10.1029/2018JC014378.
Google Scholar

Timmermans, M-L, Toole, J, Krishfield, R. 2018. Warming of the interior Arctic Ocean linked to sea ice losses at the basin margins. *Science Advances* 4(8): eaat6773. DOI: http://dx.doi.org/10.1126/sciadv.aat6773.
Google Scholar

Tippenhauer, S, Karam, S, Heuzé, C, Rabe, B. 2021. Overview on physical oceanography measurements during POLARSTERN cruise PS122—MOSAiC. PANGAEA. DOI: http://dx.doi.org/10.1594/PANGAEA.936275
Google Scholar

Toole, J, Krishfield, R, Proshutinsky, A, Ashjian, C, Doherty, K, Frye, D, Hammar,

T, Kemp, J, Peters, D, Timmermans, M-L, von der Heydt, K, Packard, G, Shanahan, T. 2006. Ice-tethered profilers sample the upper Arctic Ocean. *Eos, Transactions American Geophysical Union* 87(41): 434–438. DOI: http://dx.doi.org/10.1029/2006EO410003.
Google Scholar

Toole, JM, Timmermans, M-L, Perovich, DK, Krishfield, RA, Proshutinsky, A, Richter-Menge, JA. 2010. Influences of the ocean surface mixed layer and thermohaline stratification on Arctic sea ice in the central Canada Basin. *Journal of Geophysical Research: Oceans* 115(C10). DOI: http://dx.doi.org/10.1029/2009JC005660.
Google Scholar

Toole, JMK, Krishfield, R, Woods Hole Oceanographic Institution Ice-Tethered Profiler Program. 2016. Ice-tethered profiler observations: Vertical profiles of temperature, salinity, oxygen, and ocean velocity from an Ice-tethered profiler buoy system ITP111 [dataset]. NOAA National Centers for Environmental Information. DOI: http://dx.doi.org/10.7289/v5mw2f7x. Accessed 26 May 2021.
Google Scholar

Torres-Valdés, S, Tsubouchi, T, Davey, E, Yashayaev, I, Bacon, S. 2016. Relevance of dissolved organic nutrients for the Arctic Ocean nutrient budget. *Geophysical Research Letters* 43(12): 6418–6426. DOI: http://dx.doi.org/10.1002/2016GL069245.
Google Scholar

Uhlig, C, Loose, B. 2017. Using stable isotopes and gas concentrations for independent constraints on microbial methane oxidation at Arctic Ocean temperatures. *Limnology and Oceanography Methods* 15(8): 737–751. DOI: http://dx.doi.org/10.1002/lom3.10199.
Google Scholar

Untersteiner, N, Thorndike, AS, Rothrock, DA, Hunkins, KL. 2009. AIDJEX revisited: A look back at the U.S.-Canadian Arctic ice dynamics joint experiment 1970–78. *Arctic* 60(3). DOI: http://dx.doi.org/10.14430/arctic233.
Google Scholar

Verdugo, J, Damm, E, Nikolopoulos, A. 2021. Methane cycling within sea ice: Results from drifting ice during late spring, north of Svalbard. *The Cryosphere* 15: 2701–2717. DOI: http://dx.doi.org/10.5194/tc-15-2701-2021.
Google Scholar

von Appen, W-J, Wekerle, C, Hehemann, L, Schourup-Kristensen, V, Konrad, C, Iversen, MH. 2018. Observations of a submesoscale cyclonic filament in the marginal ice zone. *Geophysical Research Letters* 45(12): 6141–6149. DOI: http://dx.doi.org/10.1029/2018GL077897.
Google Scholar

Wassmann, P. 2015. Overarching perspectives of contemporary and future ecosystems in the Arctic Ocean. *Progress in Oceanography* 139: 1–12. DOI: http://dx.doi.org/10.1016/j.pocean.2015.08.004.
Google Scholar

Weatherall, P, Tozer, B, Arndt, JE, Bazhenova, E, Bringensparr, C, Castro, C, Dorschel, B, Ferrini, V, Hehemann, L, Jakobsson, M, Johnson, P, Ketter, T, Mackay, K, Martin, T, Mayer, L, McMichael-Phillips, J, Mohammad, R, Nitsche, F, Sandwell, D, Viquerat, S. 2020. The gebco_2020 grid—A continuous terrain model of the global oceans and land. British Oceanographic Data Centre, National Oceanography Centre, NERC, UK. DOI: http://dx.doi.org/10.5285/a29c5465-b138-234d-e053-6c86abc040b9.
Google Scholar

Wilson, C, Aksenov, Y, Rynders, S, Kelly, SJ, Krumpen, T, Coward, AC. 2021. Significant variability of structure and predictability of Arctic Ocean surface pathways affects basin-wide connectivity. *Communications Earth & Environment* 2(1): 164. DOI: http://dx.doi.org/10.1038/s43247-021-00237-0.
Google Scholar

Woodgate, RA. 2018. Increases in the Pacific inflow to the Arctic from 1990 to 2015, and insights into seasonal trends and driving mechanisms from year-round Bering Strait mooring data. *Progress in Oceanography* 160: 124. DOI: http://dx.doi.org/10.1016/j.pocean.2017.12.007.

Google Scholar

Yamamoto-Kawai, M, McLaughlin, FA, Carmack, EC. 2011. Effects of ocean acidification, warming and melting of sea ice on aragonite saturation of the Canada Basin surface water. ***Geophysical Research Letters*** **38(3). DOI:** http://dx.doi.org/10.1029/2010GL045501.

Google Scholar

How to cite this article: Rabe, B, Heuzé, C, Regnery, J, Aksenov, Y, Allerholt, J, Athanase, M, Bai, Y, Basque, C, Bauch, D, Baumann, TM, Chen, D, Cole, ST, Craw, L, Davies, A, Damm, E, Dethloff, K, Divine, DV, Doglioni, F, Ebert, F, Fang, Y-C, Fer, I, Fong, AA, Gradinger, R, Granskog, MA, Graupner, R, Haas, C, He, H, He, Y, Hoppmann, M, Janout, M, Kadko, D, Kanzow, T, Karam, S, Kawaguchi, Y, Koenig, Z, Kong, B, Krishfield, RA, Krumpen, T, Kuhlmey, D, Kuznetsov, I, Lan, M, Laukert, G, Lei, R, Li, T, Torres-Valdés, S, Lin, L, Lin, L, Liu, H, Liu, N, Loose, B, Ma, X, MacKay, R, Mallet, M, Mallett, RDC, Maslowski, W, Mertens, C, Mohrholz, V, Muilwijk, M, Nicolaus, M, O'Brien, JK, Perovich, D, Ren, J, Rex, M, Ribeiro, N, Rinke, A, Schaffer, J, Schuffenhauer, I, Schulz, K, Shupe, MD, Shaw, W, Sokolov, V, Sommerfeld, A, Spreen, G, Stanton, T, Stephens, M, Su, J, Sukhikh, N, Sundfjord, A, Thomisch, K, Tippenhauer, S, Toole, JM, Vredenborg, M, Walter, M, Wang, H, Wang, L, Wang, Y, Wendisch, M, Zhao, J, Zhou, M, Zhu, J. 2022. Overview of the MOSAiC expedition: Physical oceanography. *Elementa: Science of the Anthropocene* 10(1). DOI: https://doi.org/10.1525/elementa.2021.00062

Domain Editor-in-Chief: Jody W. Deming, University of Washington, Seattle, WA, USA

Associate Editor: Mary-Louise Timmermans, Department of Geology and Geophysics, Yale University, New Haven, CT, USA

Knowledge Domain: Ocean Science

Part of an Elementa Special Feature: The Multidisciplinary Drifting Observatory for the Study of Arctic Climate (MOSAiC)

Supplementary data

supplement - pdf file

ELEMENTA
Science of the Anthropocene

All Articles
Recently Published
Alerts
Submit
Editorial Team
Contact Us

Submission Guidelines
Publication Fees
Journal Policies
About

Online ISSN 2325-1026

STAY INFORMED

Sign up for eNews

VISIT THE UC PRESS BLOG

DISCIPLINES

Ancient World
Anthropology
Art
Communication
Criminology & Criminal Justice
Film & Media Studies
Food & Wine
History
Music
Psychology
Religion
Sociology
Browse All Disciplines

COURSES

Browse All Courses

PRODUCTS

Books
Journals

RESOURCES

Book Authors
Booksellers
Instructions
Journal Authors
Journal Editors
Librarians
Media & Journalists

SUPPORT US

Endowments
Membership
Planned Giving
Supporters

ABOUT UC PRESS

Careers
Location
Press Releases
Seasonal Catalog

CONTACT US

Acquisitions Editors
Customer Service
Exam/Desk Requests
Media Inquiries
Print-Disability
Rights & Permissions
Royalties
UC Press Foundation